INDEX

UNCLASSIFIED

Prepared under

Contract NASW-1221
National Aeronautics and
Space Administration
Washington, D.C.

ANALYZATION, DESIGN, FABRICATION, AND TESTING OF A FOIL BEARING ROTOR SUPPORT SYSTEM

Quarterly Technical Report
Period Ending February 21, 1966

RR66-8

March 21, 1966

Copy____Of____

Albert F Stuller Date 18 March '66
Prepared By

Approved By Date 18 March '66

V-E Rayossine Date March 23, 1966
Approved By

AMPEX CORPORATION

RESEARCH AND ENGINEERING PUBLICATION

UC-270

ABSTRACT I

The fabrication of the high-speed, self-acting, gas lubricated, foil bearing, rotor support test rig has been completed. This test rig is being designed for a maximum rotational speed of 570,000 rpm, and it is instrumented to continuously measure shaft speed, shaft motion in two planes, foil tension and wrap angle, and the torque exerted by the rotating shaft on the foil journal bearing. The construction of this test rig is complete. Testing has shown that the rotor is free from half-frequency whirl instability at rotation speed up to 240,000 rpm.

A study of the stress and vibration characteristics of high speed rotors showed that rotor designs are often limited by the first free-free bending critical speed because conventional gas lubricated bearings cannot support a shaft during acceleration through this critical speed.

Three rotors supported on self-acting gas lubricated journal bearings were accelerated up to a rotational speed corresponding to their free-free critical speed. The speed and shaft orbital motion data were recorded on magnetic tape. It was not possible to rotate these shafts at speeds in excess of their free-free critical speeds. There was no damage to either the shaft or to the foil journal bearings after operation at this critical speed.

No signs of half-frequency whirl instability were observed during the operation of a shaft 5/8 in. in diameter by 4.5 in. long supported by helium lubricated self-acting foil journal bearings at rotational speeds from zero to 360,000 rpm. However, at certain speeds the shaft acquired a low frequency motion which corresponded to the natural frequency of the shaft supported on the Havar* foil.

*Trade Mark, Hamilton Watch Company

ABSTRACT I (Continuation)

During operation of the high-speed test rig (1 in-diameter shaft) low frequency shaft motion was observed. This was found to vary as a function of foilwrap angle and foil tension. The analysis of foil bearings has been extended further. Steady state conditions were considered and it was found that a single foil system's attitude angle is not necessarily zero. It was also found that, in the first approximation, the attitude angle of a three-foil system is zero.

ABSTRACT II

During the last reporting period, test data was taken on the high speed test rig (1 in-diameter shaft) exclusively. This unit was run with both air and helium. All test data - shaft speed, orbital motion, and dynamometer torque - were recorded on magnetic tape. As with the smaller test rig, 5/8 in. diameter, low frequency motion was observed with the larger, high-speed unit. The low frequency whirls were found to change as foil wrap angle and foil tension were varied. The highest speed recorded with this test unit was 240,000 rpm on helium. The largest amplitude orbit, 0.001 in., was found at this speed. It is believed this large amplitude and some of the low frequency motions are associated with the thrust bearing. Also during the last reporting period the analysis of foil bearings was extended.

In Appendix I, the results of a preliminary investigation into the question of the attitude angle of foil bearings are described. Only steady state conditions are considered. It is found that, contrary to previous expectations, a single foil system has an attitude angle which is not necessarily zero. Specific cases are analyzed. It is further found that for a symmetrically situated 3-foil system, the attitude angle is, nevertheless, zero to the first approximation.

CONTENTS

LIST OF FIGURES

LIST OF FIGURES (Continued)

LIST OF FIGURES (Continued)

NOMENCLATURE

C	Radial clearance (in.)
E	Young's modulus of elasticity ($lb/in.^2$)
F	Centering force (lb/in.)
K	Positional stiffness (lb/in./in.)
K_B	Lubricating film stiffness (lb/in./in.)
K_F	Foil positional stiffness (lb/in.)
P	Pressure (psi)
P_a	Ambient pressure (psi)
R	Radius (in.)
T	Foil tension (lb/in.)
U	Velocity (in/sec)
Z	Rectangular coordinate
e	Eccentricity (in.)
f	Frictional force (lb/in.)
h	Lubricating film thickness (in.)

ℓ	Foil length (in.)
t	Foil thickness (in.)
Λ	Compressibility number
α	Whirl angular speed ($d\alpha/dt$)
θ	Wrap angle (radians)
μ	Viscosity (lb-sec/in.^{2})
ξ	Z/R
ω	Angular velocity (radians/sec)

ANALYZATION, DESIGN, FABRICATION, AND TESTING OF A FOIL BEARING ROTOR SUPPORT SYSTEM

1.0 INTRODUCTION

A foil bearing is a fluid bearing in which one member is flexible. Foil bearings differ from conventional bearings in which both surfaces are rigid, in that the flexibility of one member causes the pressure within the bearing to be almost constant. To illustrate this, the pressure distribution in a conventional self-acting bearing and a self-acting foil bearing, each subtending an arc of 120°, is shown in Fig. 1. The pressure distribution in a bearing with rigid surfaces can be found in most standard texts on lubrication[1], and the pressure distribution of a self-acting foil bearing is described in reference 2. The force and displacement vectors of the same two bearings are also shown in Fig. 1. It can be seen that for the bearing with rigid surfaces, the misalignment between these two vectors is about 25°, while it is less than 5° for the foil bearing.

From Fig. 1 it can be seen that for the bearing with rigid surfaces, the resultant of the fluid film forces has a component which is tangential to the surface of the bearing. It is this tangential component which causes whirl of the rotor. All fluid film bearings, in which this tangential component is present, have a tendency to whirl. Since the lubricant between the rotating shaft and the stationary boundaries moves at approximately one-half the rotational speed of the shaft and the shaft must displace the fluid if it is to whirl, this self-excited whirl usually takes place at approximately one-half the rotational speed of the shaft. This whirl tendency is aggravated when there is little damping; i.e., when the lubricant is a low viscosity fluid such as gas or a liquid metal.

If it is assumed that the frequency and amplitude of any whirling motion are constant, the load capacity of a cylindrical gas lubricated journal bearing can be obtained from the Reynolds equation for isothermal flow[1]. See Fig. 2.

$$\frac{\partial}{\partial\theta}\left[\left(\frac{h}{C}\right)^3 P\frac{\partial P}{\partial\theta}\right]+\frac{\partial}{\partial\xi}\left[\left(\frac{h}{C}\right)^3 P\frac{\partial P}{\partial\xi}\right]=\Lambda\left(1-\frac{2\dot{\alpha}}{\omega}\right)P_a\frac{1}{C}\left(\frac{\partial(hP)}{\partial\theta}\right)$$

$$\xi = z/R$$

$$h = C+e\cos\theta \qquad (1)$$

$$\Lambda = \frac{6\mu UR}{P_a C^2}$$

The right-hand side of Eq. (1) describes the driving function and, together with the diffusion terms on the left-hand side, determines the load capacity of the bearing. This equation assumes isothermal flow of a Newtonian fluid between perfectly smooth rigid surfaces.

From the equation it can be seen that whenever $\dot{\alpha}$, the whirl velocity is one-half the spin velocity, ω, the load capacity goes to zero because $(1-\frac{2\dot{\alpha}}{\omega})$ goes to zero. When this occurs, failure usually results due to the occurence of the half-frequency whirl instability which determines the maximum speed and/or operating conditions of most conventional, self-acting, gas lubricated journal bearings.

However, in self-acting foil journal bearings, the resultant fluid film force may have a small tangential component, i.e., zero attitude angle, and therefore no tendency to whirl. It is this characteristice of the self-acting foil bearing that makes it particularly attractive for high-speed rotor support applications. Analytical and experimental investigation of self-acting foil journal bearings will be made to determine the magnitude of this attitude angle.

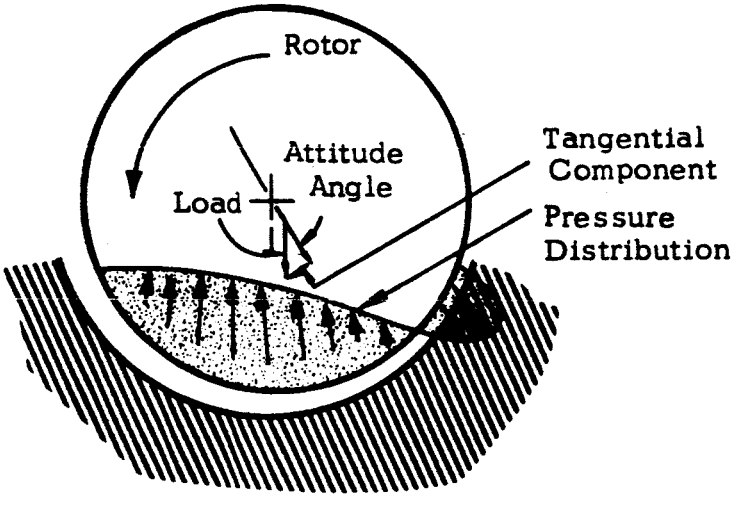

Self-Acting Rigid Surface Bearing

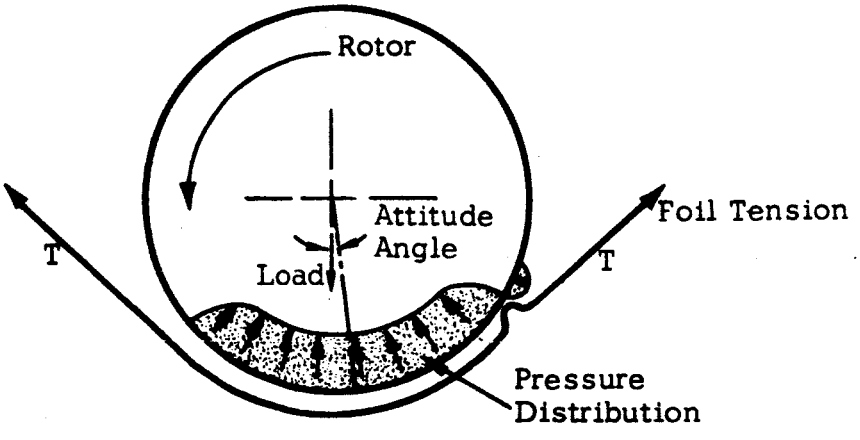

Self-Acting Foil Bearing

Fig. 1 Load, Attitude Angle, and Pressure Distribution in Self-Acting, Rigid Surface Bearing and Foil Bearing

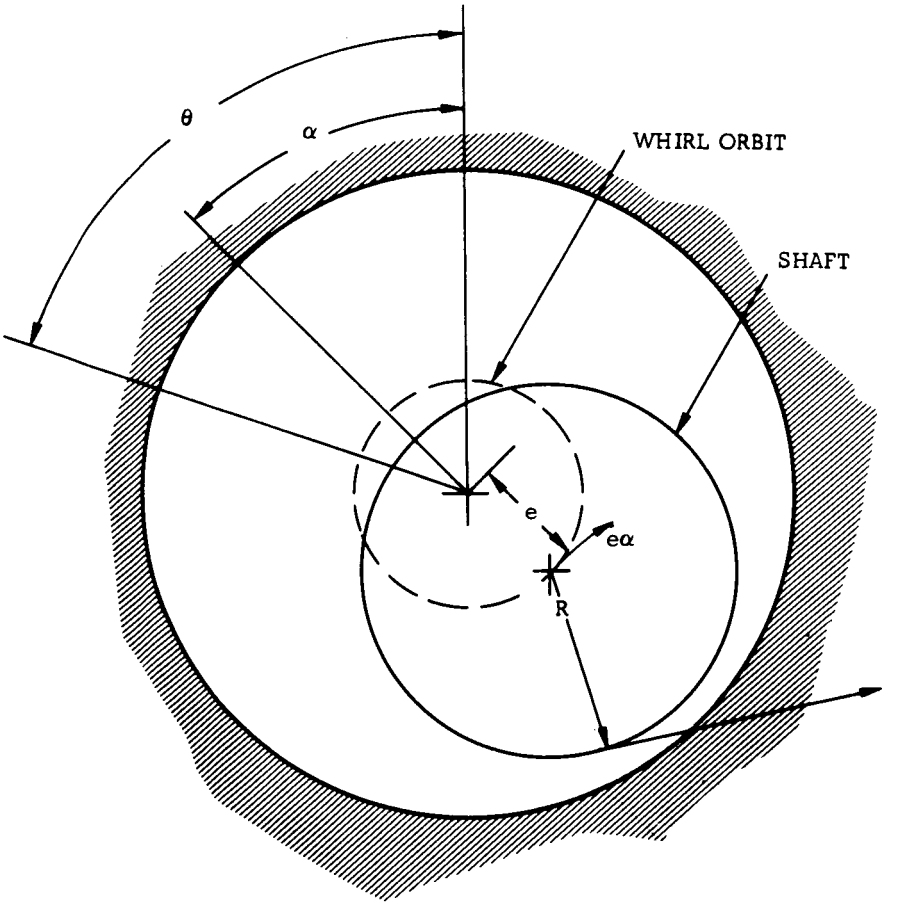

Fig. 2. Schematic Diagram of a Journal Bearing in Circular Whirl

2.0 OBJECTIVES

The objectives of this study are to determine by analytical and experimental means the characteristics and limits of applicability of high-speed rotor supports using self-acting, gas-lubricated, foil journal bearings. This work is segmented into three major categories:

(a) The analysis of a self-acting gas lubricated foil bearing rotor support system consisting of three symmetrical steel foils operated in an inert gas atmosphere;

(b) The design and fabrication of a self-acting, gas-lubricated, foil journal bearing rotor support system;

(c) The test of this rotor support system with the primary emphasis on the determination of the maximum speed at which the rotor can be operated without encountering self-excited "whirl" instability.

NOTE:

The information included in the part progress reports has not been deleted. To provide continuity, information presented in earlier reports has been updated. The work accomplished during this reporting period is described on pages 27, 33 and 50.

3.0 PROGRAM DESCRIPTION

The self-acting, gas-lubricated foil journal bearing has been used to support rotors at speeds in excess of one-quarter million rpm . The apparent absence of half-frequency whirl instability in this type of journal bearing has made it attractive for use in high-speed applications or under the conditions of light load, particularly such as would be found in a space environment. There are, however, some undesirable characteristics associated with foil journal bearings. These bearings obtain their freedom from self-excited, half-frequency whirl from the flexibility of the foil; it is this flexibility which creates many of the problems that have prevented their use in practical applications.

There are four major problem areas associated with the support of high speed-rotors on gas lubricated self-acting foil journal bearings:

(1) The possibility of a limited rotational speed due to the occurence of self-excited, half-frequency whirl instability;

(2) The high starting torque resulting from the "capstan effect";

(3) The low frequency critical speeds associated with the mass of the rotor and the small positional stiffness of the foil journal bearings;

(4) Structural limitations which, thus far, have prevented the operation of rotors supported on gas lubricated journal bearings beyond their first free-free bending critical speed.

These four problem areas can be roughly separated into three categories:

1. High speed investigations
2. Low speed investigations
3. Flexural critical speed investigations

The objectives of this program will be best satisfied where test equipment for each of the areas of investigation is designed specifically for testing in that area rather than using a single piece of test equipment for all studies.

3.1 High Speed Test Rig

The fabrication of the high-speed, self-acting, gas-lubricated, foil bearing, rotor support test rig has been completed. The rig is designed for a maximum shaft speed of 570,000 rpm. The speed of the shaft is limited by two factors: radial and tangential stresses which would cause the shaft to burst and the first free-free flexural critical speed. The effects of shaft length and diameter on these two criteria are shown in Fig. 3. It can be seen that very high rotational speeds are limited to short, small-diameter rotors. The design point shown in this illustration represents a compromise between high speed and sufficient length to allow room for instrumentation; i.e., the shaft has been designed to place its free-free and burst speeds close together and above 500,000 rpm.

During operation, continuous measurements can be made of the shaft motion and/or growth by capacitance probes located in two planes: one near each end of the shaft. Four capacitance probes are installed in each of these planes. The journal bearings used to support the shaft consist of three separate foils spaced at 120°, each having individually controlled foil tensions and wrap angles. The foil material is 1/2 in. Havar* of thicknesses varying from 0.0005 to 0.001 in.

* Trade Mark, Hamilton Watch Company

Figures 4 through 7 show the step-by-step buildup and instrumentation of the high speed test rig. The entire unit may be enclosed within a 17 in. diameter cylinder of a 6061-T6 aluminum alloy with wall one inch thick, which provides blast protection.

The radial inflow turbine which drives the rotor is located on the upper end of the rotor. The rotor is supported from below by an externally pressurized, gas lubricated thrust bearing. The foil journal bearings are located near the extreme ends of the rotor, and the planes of the capacitance measuring probes are located adjacent to these bearings. Each of the foils can be individually adjusted to change wrap angle, foil tension, and radial position. All of these parameters can be measured, either by micrometer motion, strain gage, or capacitance probe.

For present testing purposes, a simplified test rotor has been machined from Ni-Mark 300*. This material has a yield strength of over 270,000 psi. For higher speeds in air and helium, a higher efficiency and thus more complicated turbine will be machined; it has already been designed and machined into a brass shaft. Helium tanks and manifolding have been installed, but are not used until all initial adjustments have been made on air. Maximum rotational speeds attainable with air are approximately 210,000 rpm. Since helium, at room temperature and at the pressure ratio currently being used, has over eight times the adiabatic head and approximately three times the sonic velocity as compared to air, we expect to reach design speed with helium. However the present helium manifolding will have to be modified to allow a higher flow rate than is now possible.

*Trade Mark, Carpenter Steel Company

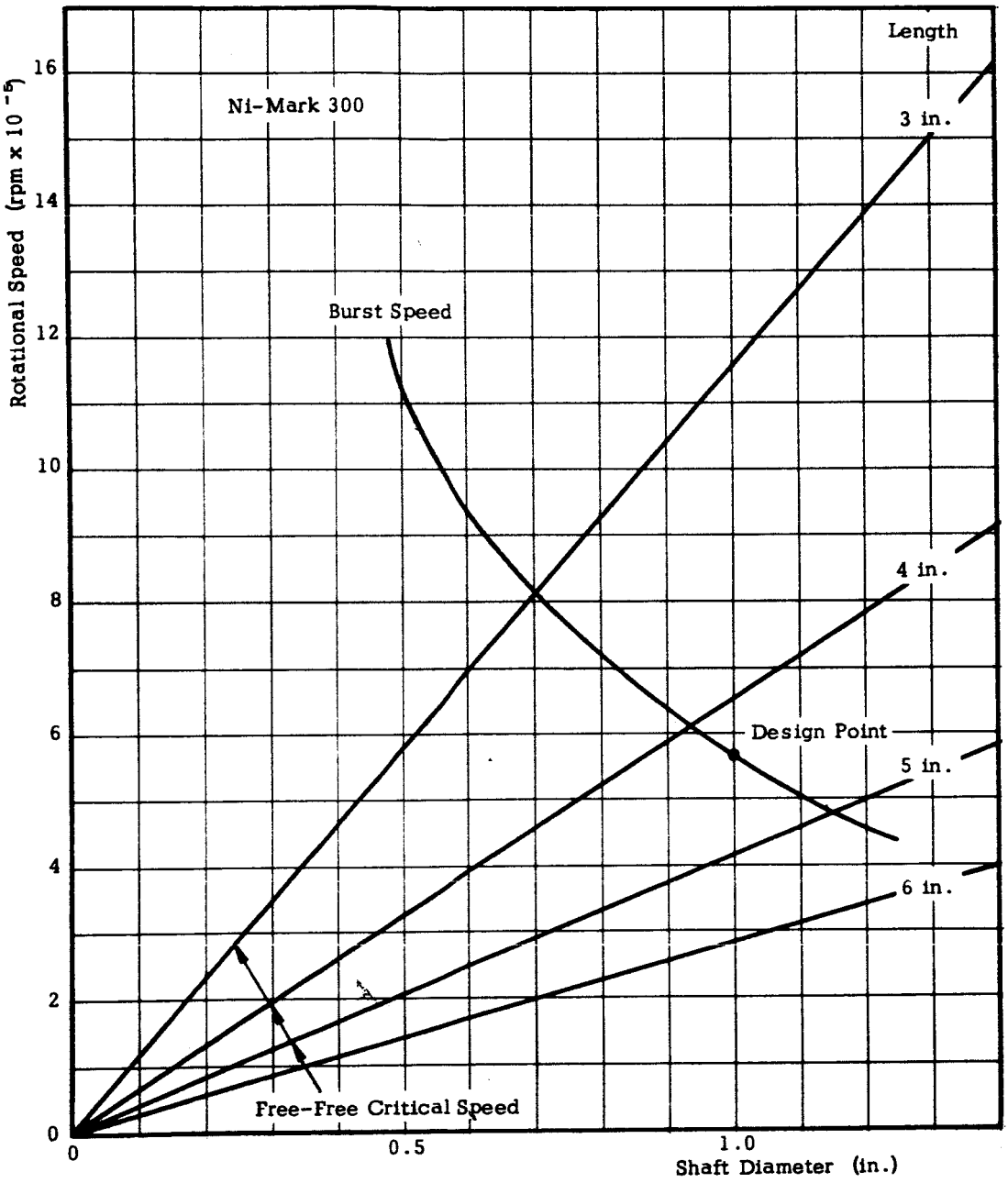

Fig. 3. Burst Speed and Flexural Vibration Characteristics of a High Speed Rotor

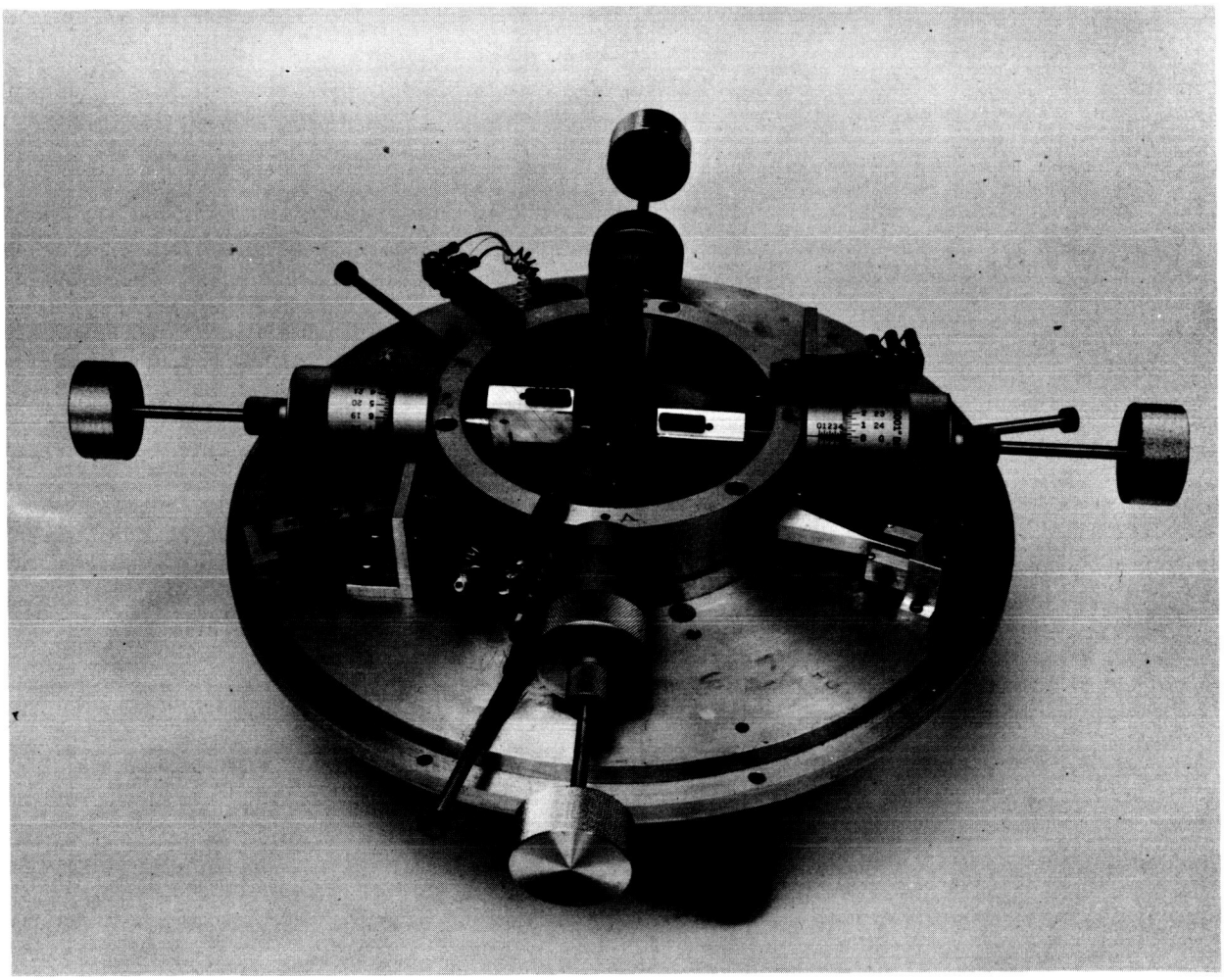

Fig. 4. High Speed Test Rig, Simplified Rotor, Dynamometer, and Lower Capacitance Probes

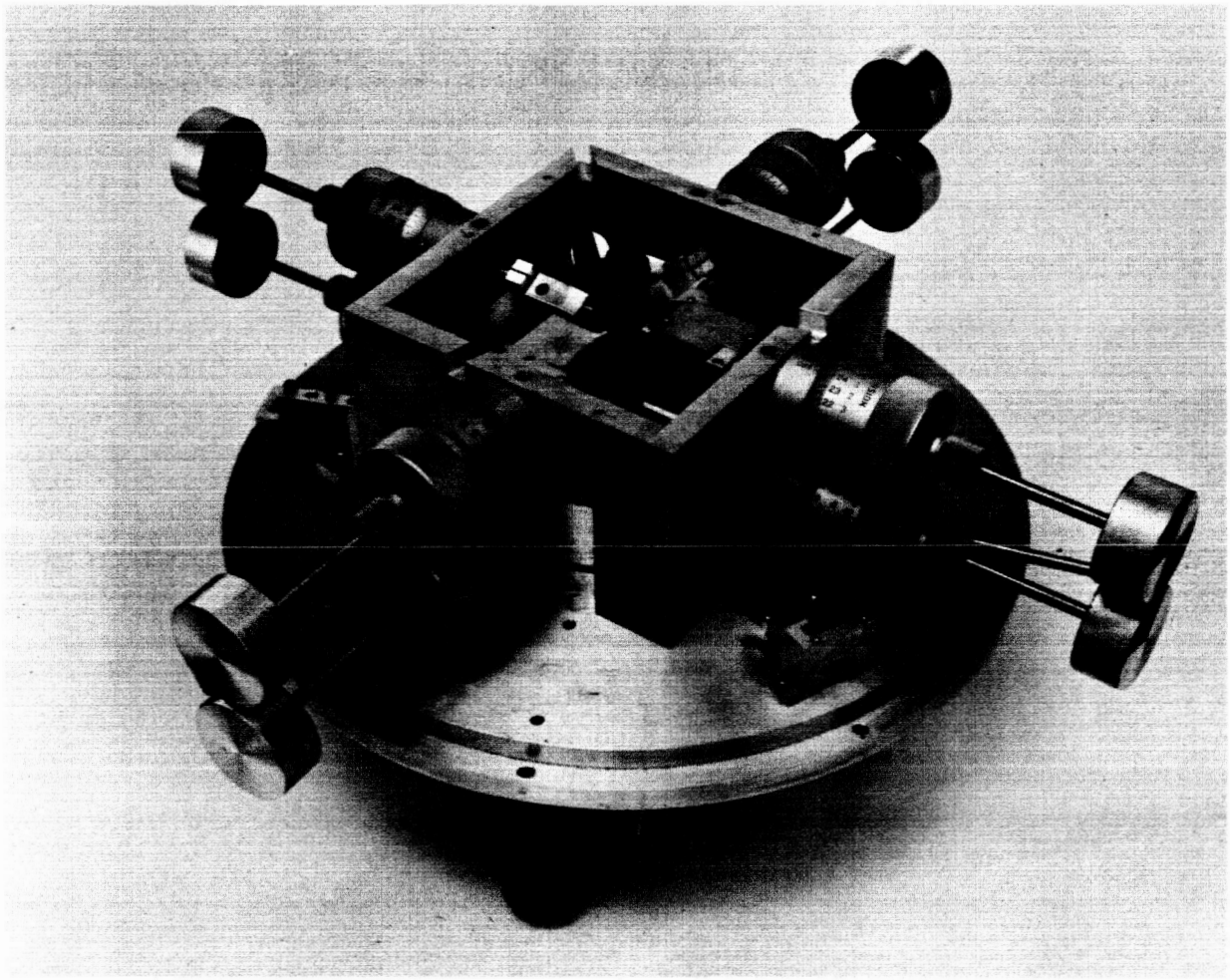

Fig. 5. High Speed Test Rig, Upper Capacitance Probes

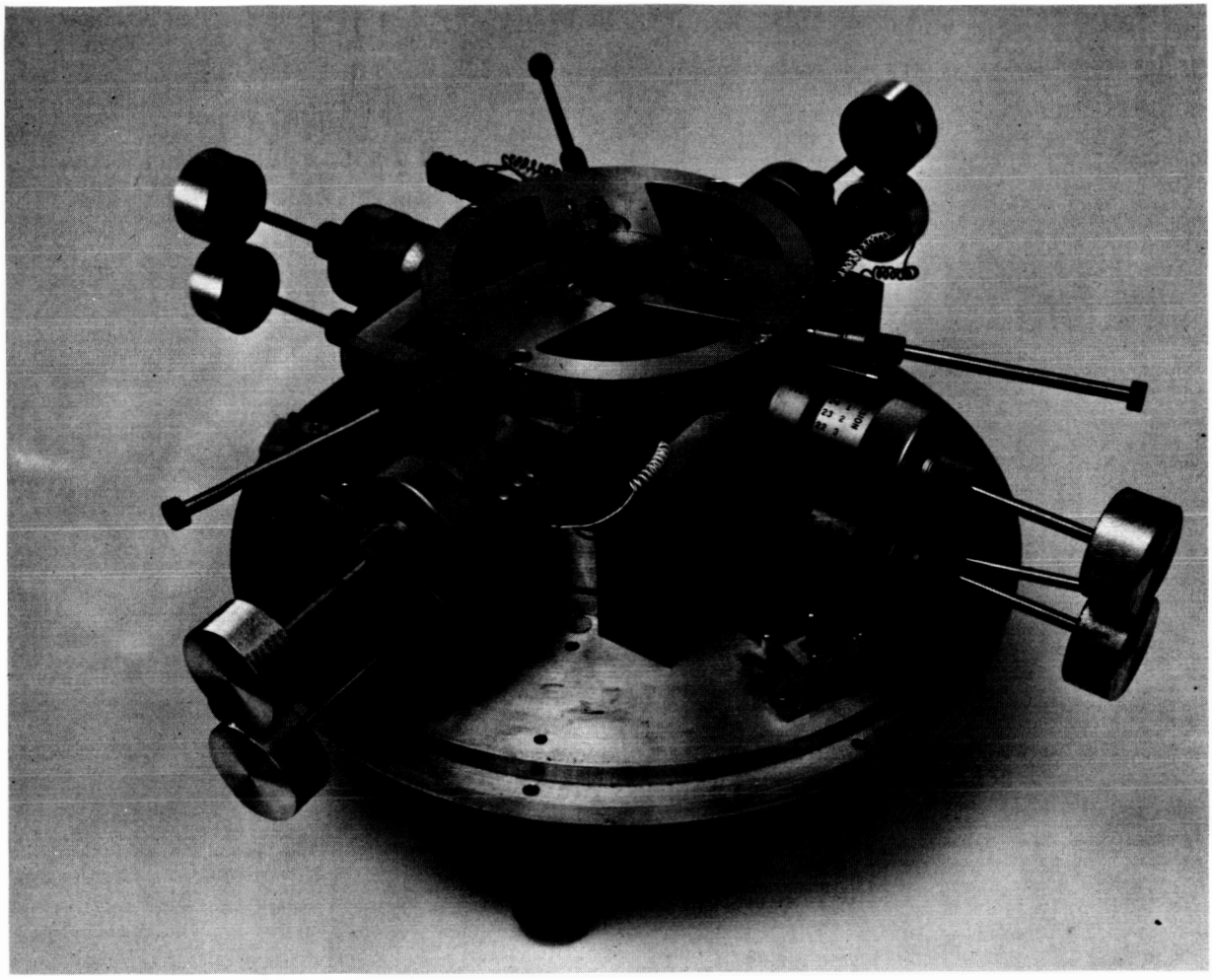

Fig. 6. High Speed Test Rig, Upper Foil Support Plate

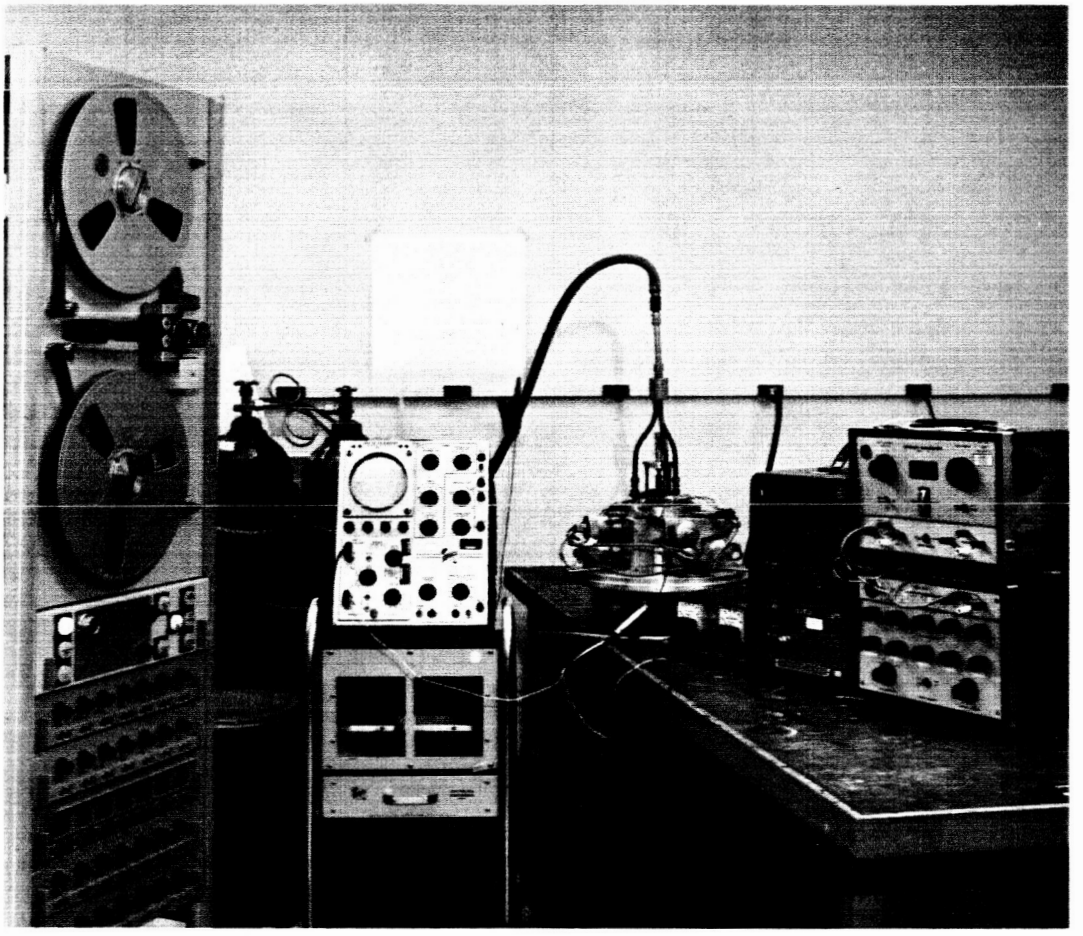

Fig. 7. High Speed Test Rig, and Instrumentation

3.1.1 Dynamometer

The dynamometer consists of an air supported circular plate upon which are mounted the foil adjuster blocks. Figure 8 is a photograph of the bottom assembly. The dynamometer plate is located in the center and is kept from rotating by a calibrated cantilever spring which can be seen at the left. The torque on the dynamometer, caused by the drag on the three bottom foils, is monitored by double ended capacitance probes. These are located on the right side of Fig. 8. Preliminary testing with the dynamometer calibration has given the data shown in Fig. 9.

3.1.2 Speed Monitor

Shaft speed is monitored by a magnetic speed pickup manufactured by Pace Engineering Company, Model SV-2. The speed pickup is a magnetic device with a high-turn coil. The sensitivity of the device allows monitoring of shaft speed even though it is placed several inches from the shaft. The output of the speed pickup is fed into an electronic counter which displays shaft speed in cycles per second.

3.1.3 Capacitance Motion Measuring Instrument

The shaft orbital motion, shaft growth, and dynamometer angular rotation are all measured by the means of capacitance probes which detect these parameters as changes in capacitance. The requirements of this measuring system are: static calibration, high sensitivity, repeatability, low noise and a wide dynamic range. The high-speed foil bearing rotor support test rig requires a minimum of nine separate channels.

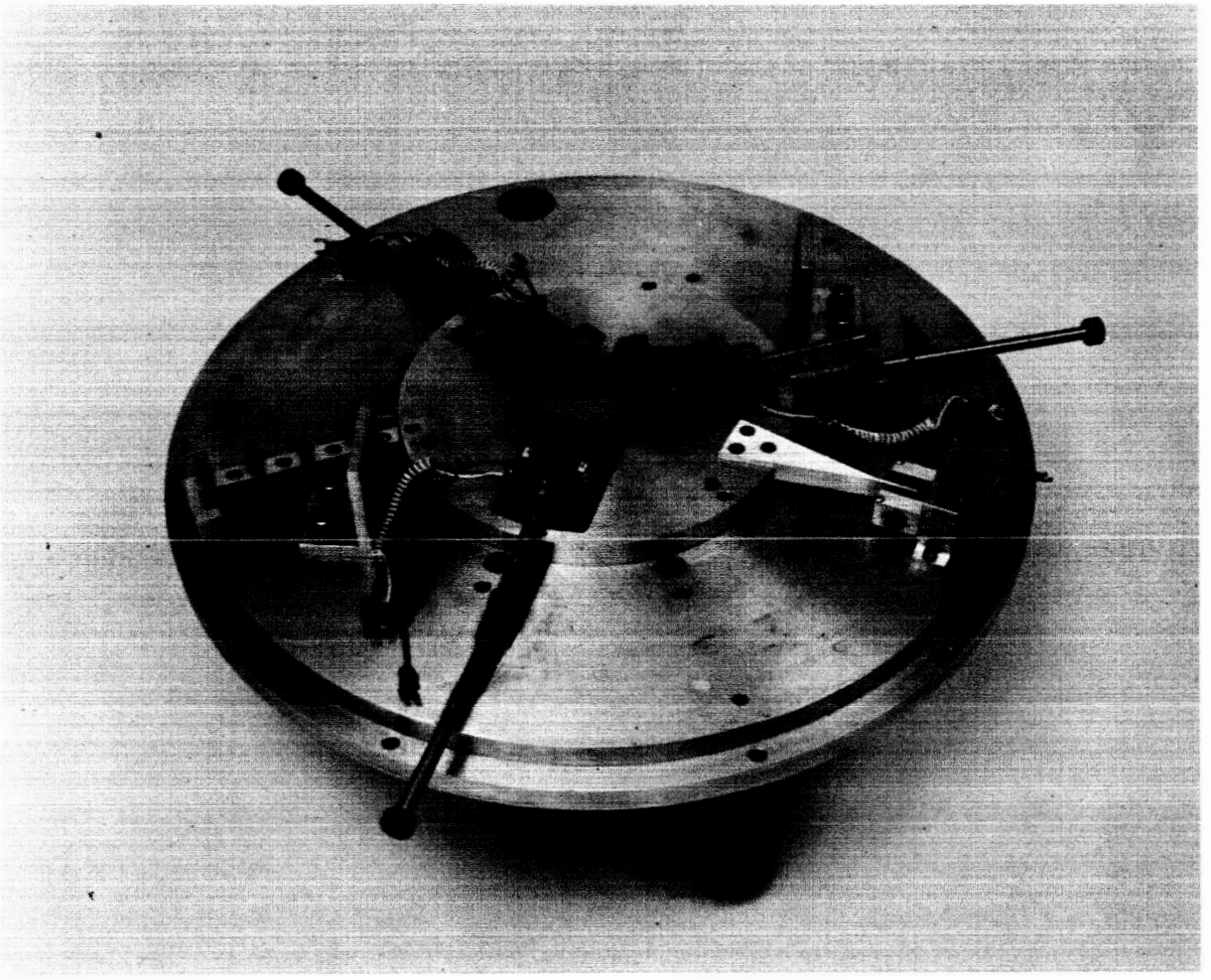

Fig. 8. High Speed Test Rig, Bottom Support Assembly

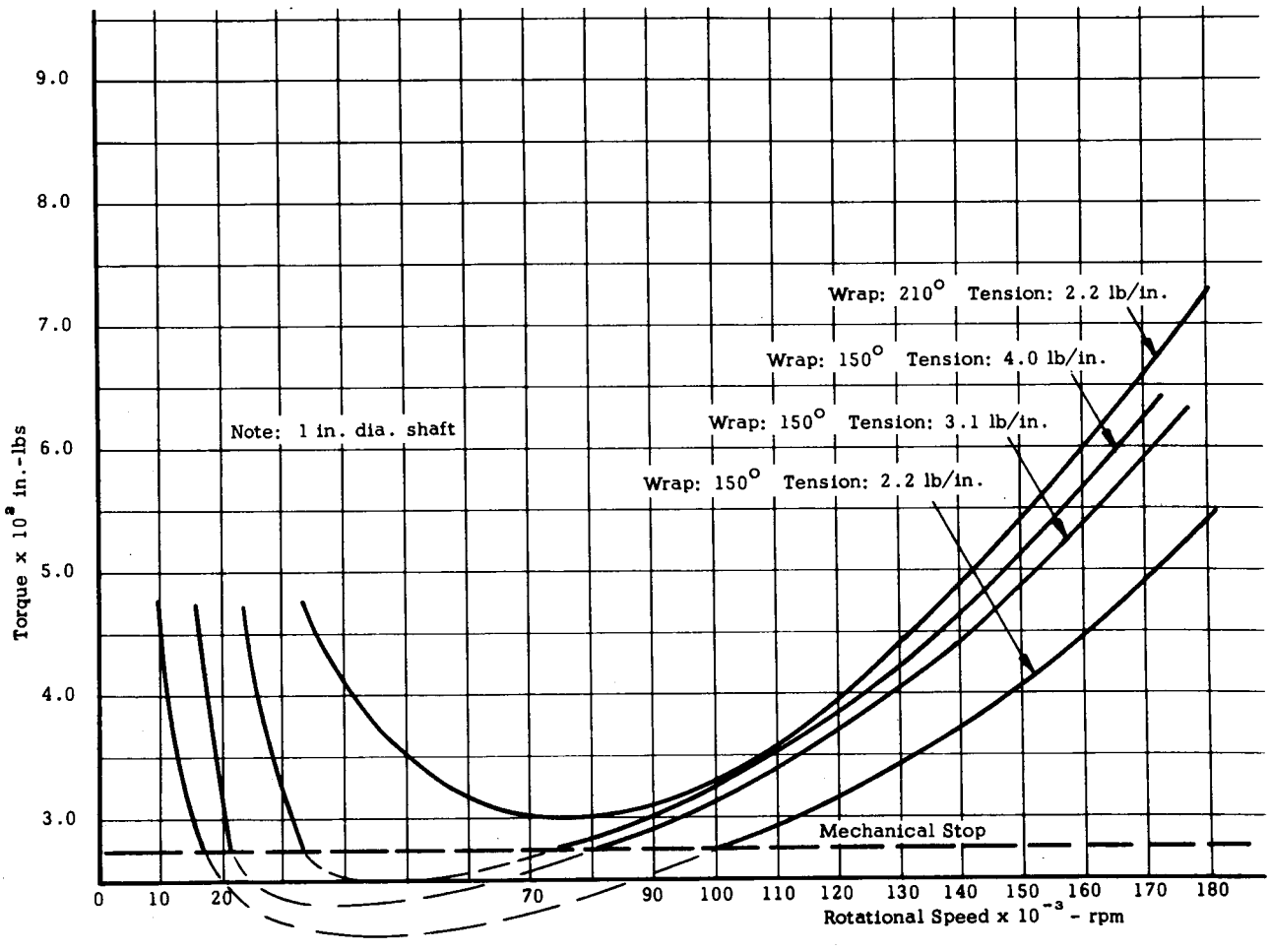

Fig. 9. Torque Variations with Speed, Wrap Angle, and Foil Tension

The Lion Research Corporation transducer system was thought to be well suited to the present application because of the small size of the detector, the low background noise and cost per channel. Figure 10 shows a calibration curve of one of the Lion Units. With a ± 0.001 in. displacement about the zero set, the output is nearly linear and the sensitivity is 0.4 volts/mil. The noise level of this unit is approximately 0.03 volt.

Figure 11 shows the measured frequency response of the Lion Research "C" Line Driver. Here it can be seen that any frequency of motion higher than 100 cycles per second is strongly attenuated. This high frequency attenuation makes the Lion unit unsuitable for monitoring orbital motion during high-speed rotor tests. To overcome this difficulty, a 1.38 megacycle rf driver and capacitance measuring probes to fit the high-speed test rig were designed and built. The design of the probes was based on the material presented in reference 3.

The frequency response of the capacitance motion detector probe and its associated electronics alone, and the frequency response of the entire system are shown in Fig. 11. The detector offers no attenuation for all practical rotational speeds, and the entire system is flat to 40 Kc and drops only by 5% at 10 Kc, which is the highest rotational speed anticipated in this test series. The probe and driver electronics are shown in Figs. 12 and 13. The noise level of the completed twelve-channel capacitance motion measuring system is less than 0.01 volt.

Figure 14 shows the wiring diagram for the capacitance probes. These probes may be used in either a single ended or push-pull configuration. Shifting from one mode of operation to the other requires only an exchange of wiring harnesses.

Figure 15 shows the calibration curve of the capacitance probes in push-pull configuration. This was the configuration used during this phase of testing.

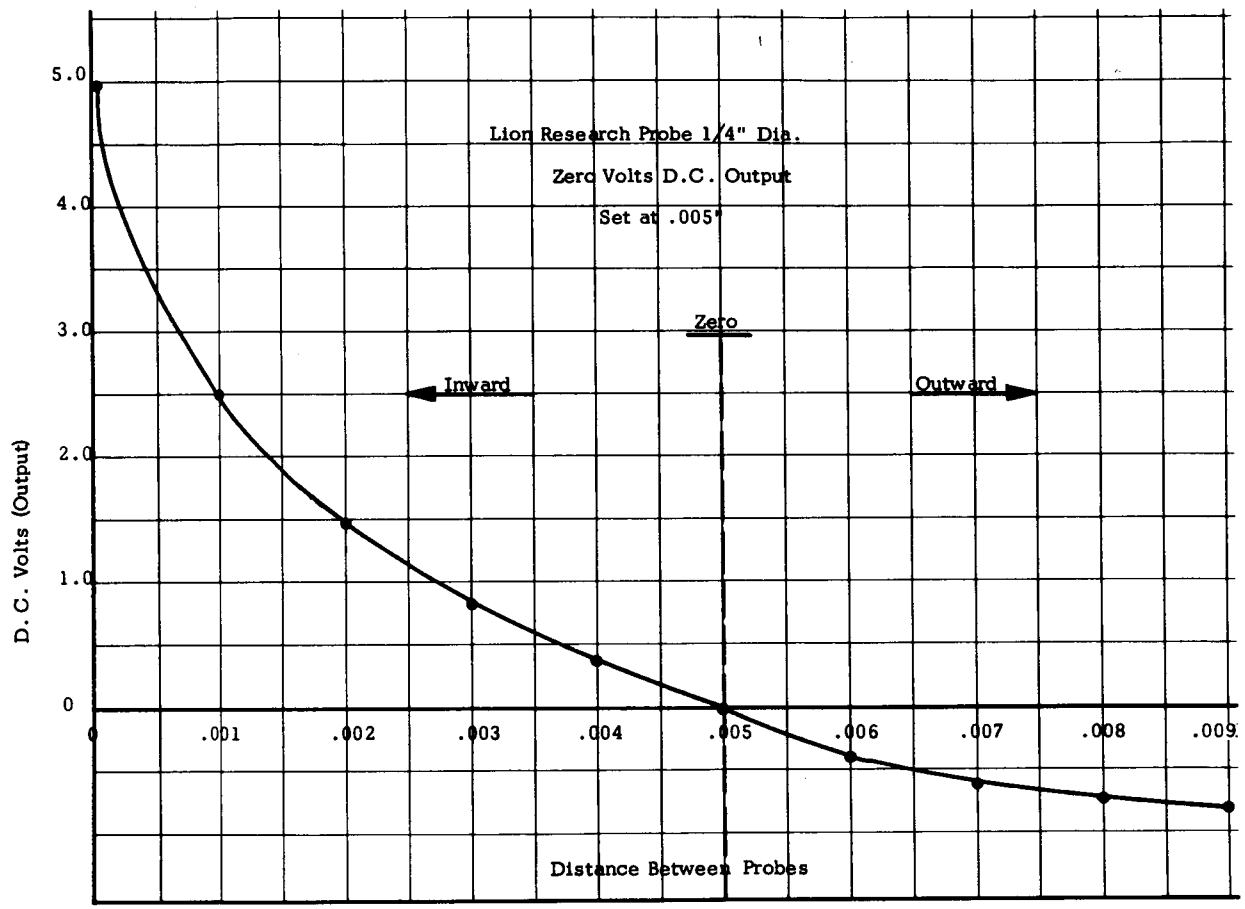

Fig 10. Calibration Curve of Lion Research Capacitance Probe Single Ended; .25 Dia., Zero Set at .005 Inches

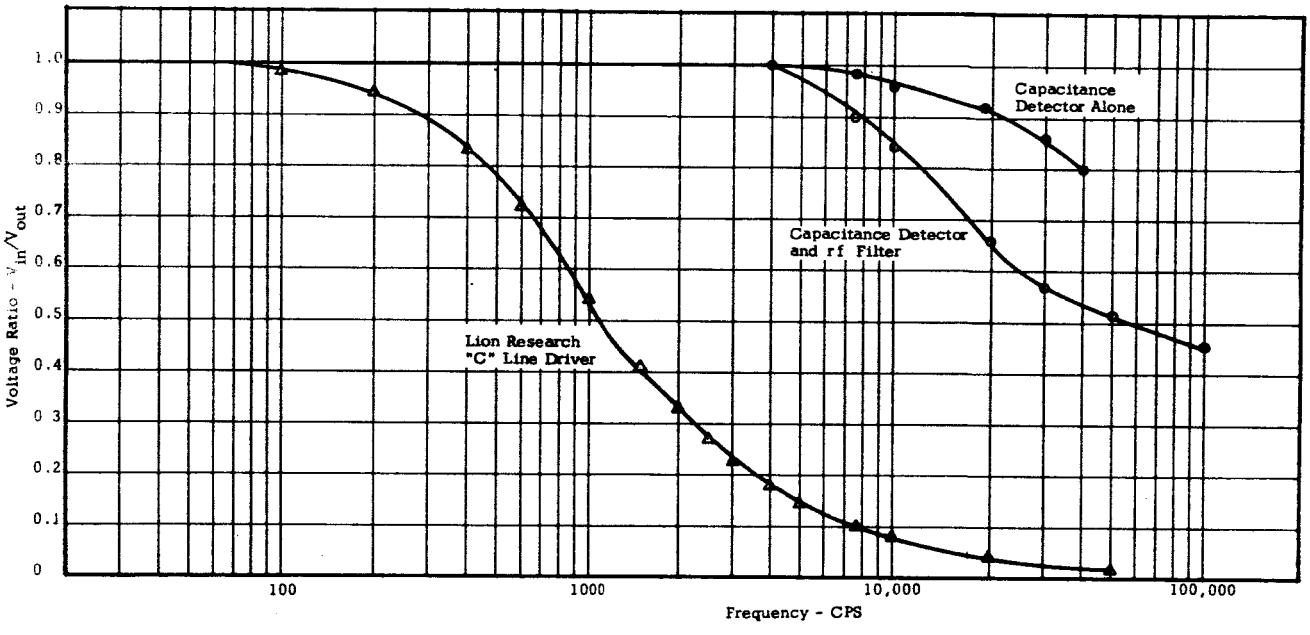

Fig. 11. Frequency Response Characteristics of Capacitance Insertion Probes

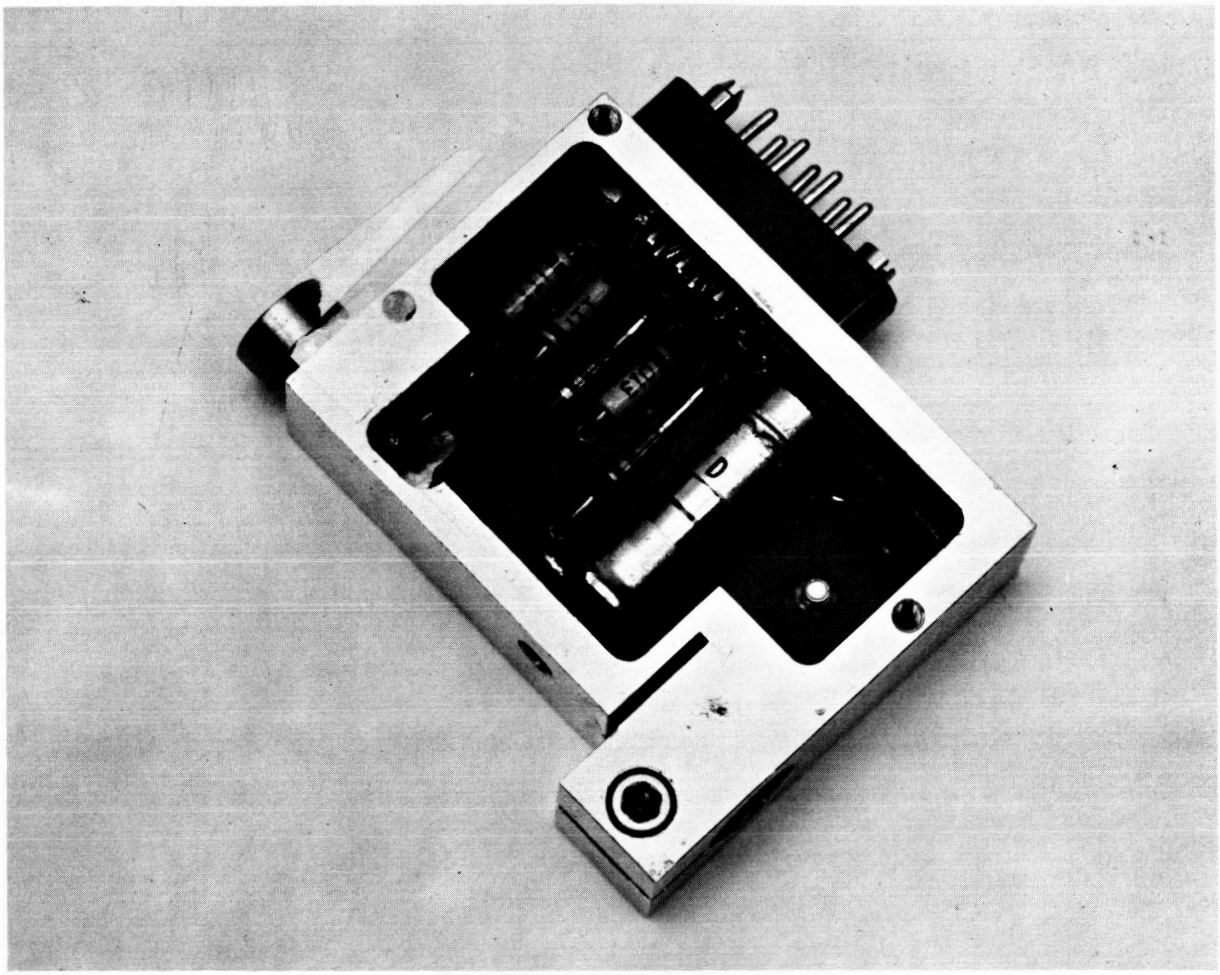

Fig. 12. Capacitance Measuring Probe and Associated Electronics

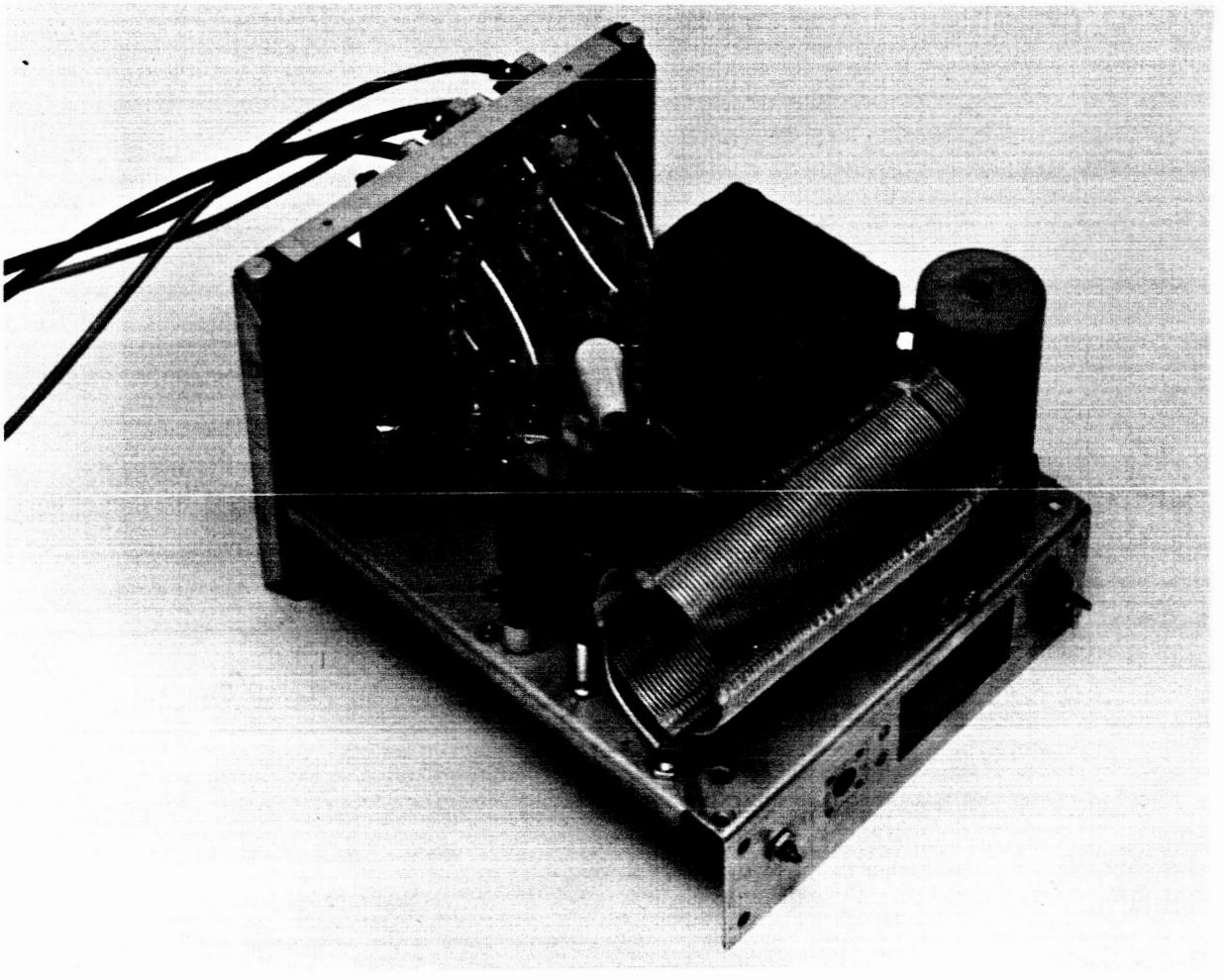

Fig. 13. Capacitance Probe Driver Electronics

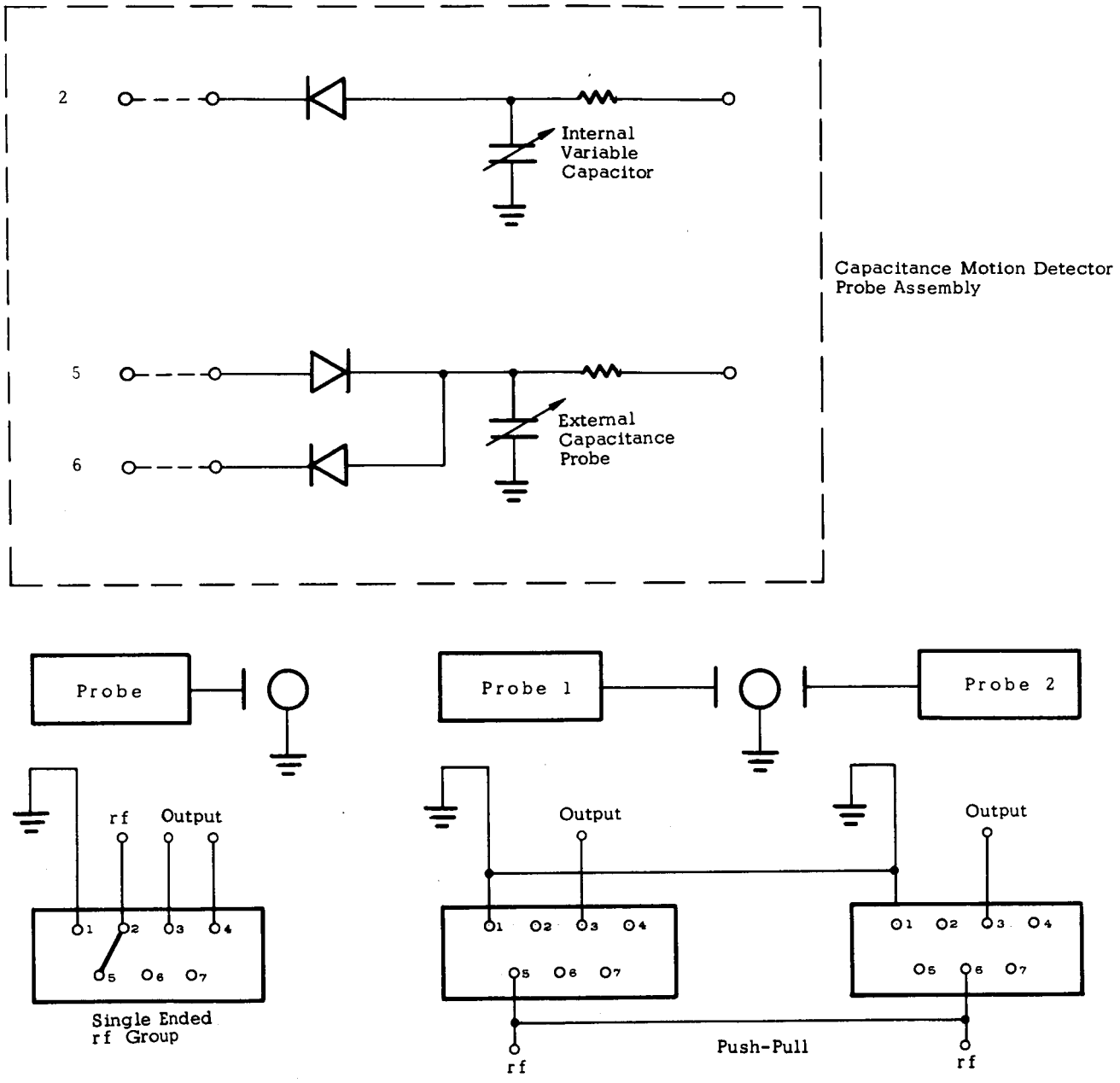

Fig. 14. Schematic Diagrams of Capacitance Motion Detector Probe and Wiring Harness

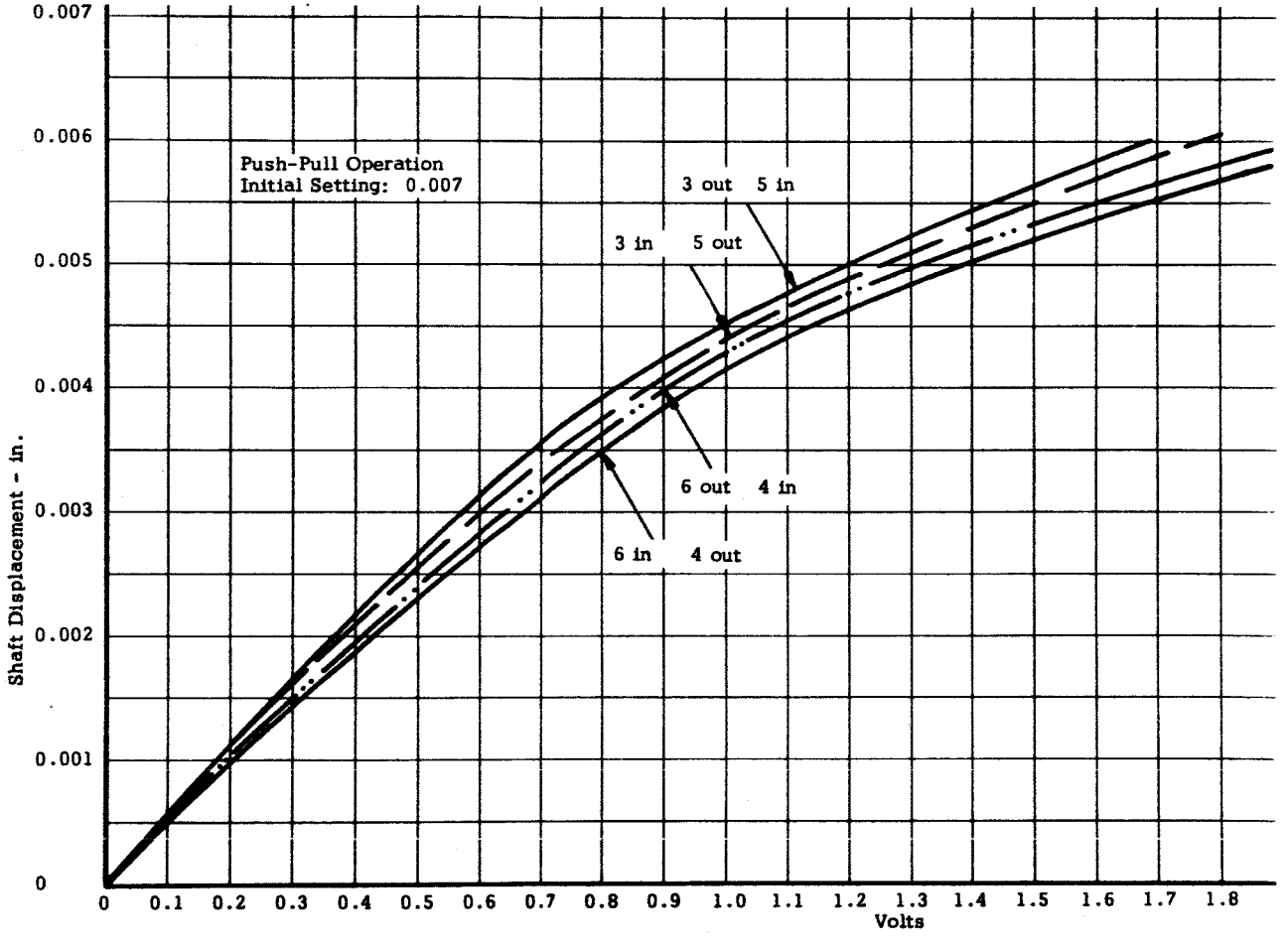

Fig. 15. Calibration Curve of the Capacitance Probes Used to Monitor Shaft Motion

3.2 Problems and Solutions

3.2.1 Strain Gage Beams

After a test of the high-speed test rig, it was found that the original aluminum beams used to measure the foil tension had taken a permanent set. This happened when the thrust bearing failed to operate correctly because of insufficient air supply, and the resultant large shaft excursion overstressed the beams. New, stronger beams were fabricated from hardened beryllium-copper. Figure 16 is a photograph of a section of the floating circular plate used as a dynamometer. In the center of the picture, the earlier aluminum strain gage beam is shown with the new one. The beryllium-copper beam is mounted on its adjuster block and with foils in place. Beryllium-copper was chosen for its characteristics of low hysteresis, low elastic modulus, and high strength. The new tension beams have been installed and the strain gages calibrated.

3.2.2 Thrust Bearing

During preliminary testing with the high speed test rig, rotor vibration was noticed. It was found that during the run, the air pressure to the thrust bearing would drop below the level required to support the shaft. This was corrected by using an independent gas supply system for the thrust bearing. The bearing itself has been modified to include a Teflon filled bronze thrust surface. Initially, speeds up to 210,000 rpm have been achieved, with no noticeable vibration. Figure 16 shows the present thrust bearing surrounded by the three bottom foils. It has been found, however, that with continuous running this bearing has not operated successfully. It is believed to be the

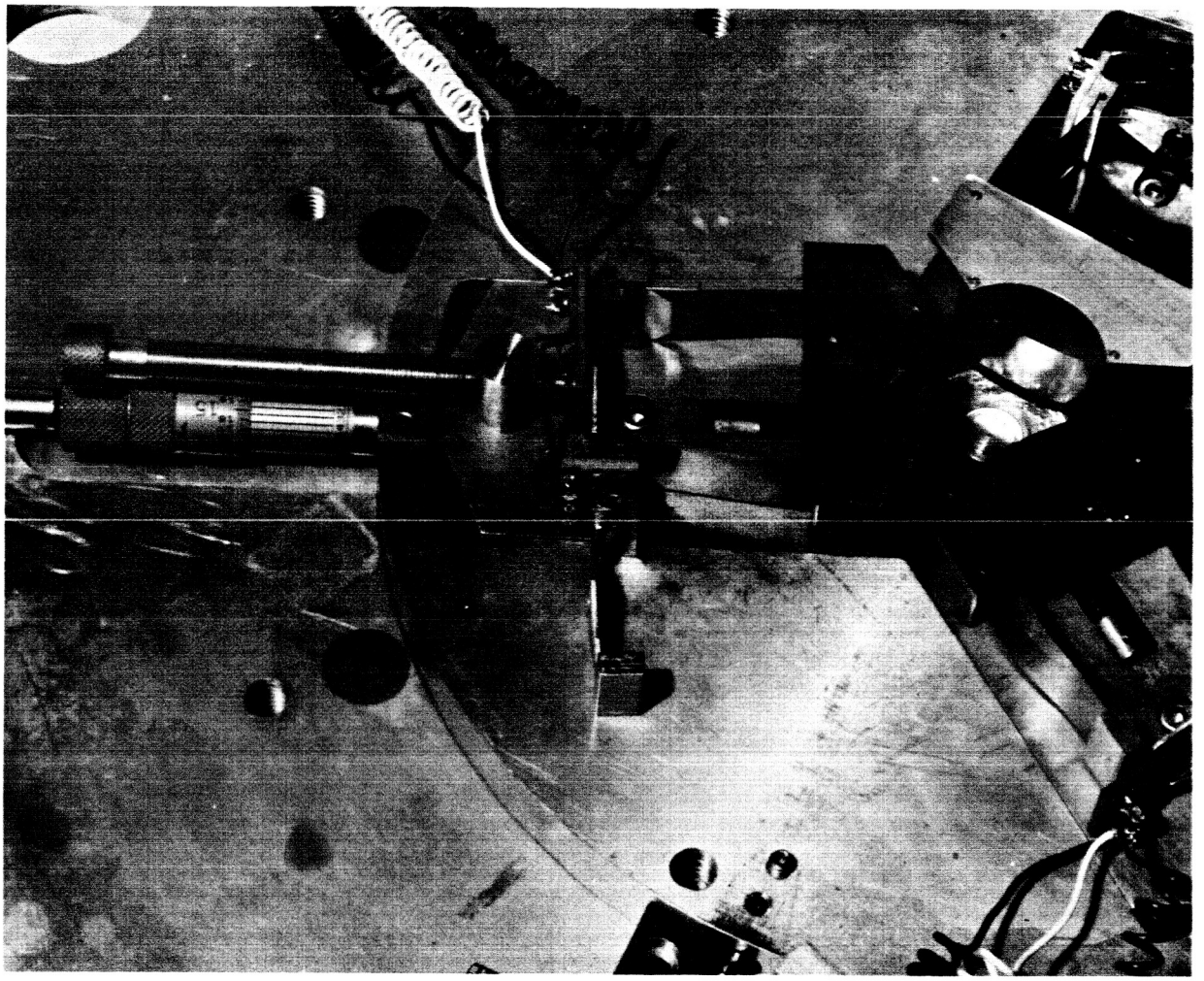

Fig. 16. High Speed Test Rig, Dynamometer, Plate Assembly

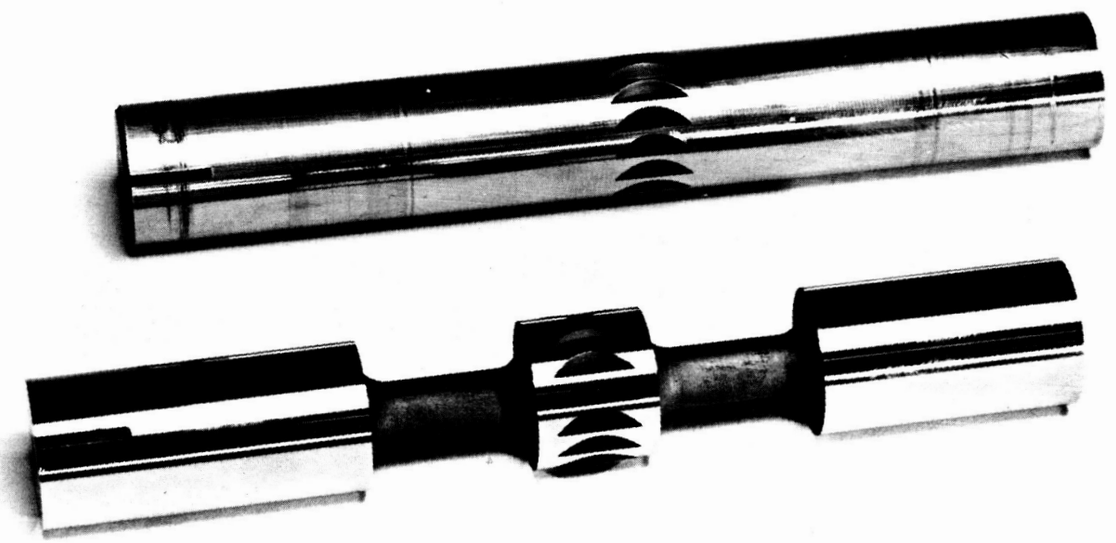

Fig. 17 Flexural Shafts with Free-Free Critical Speeds of 100,000 rpm and 336,000 rpm

cause of some of the low frequency shaft motions. For high speed runs on helium, a redesigned thrust bearing of greater load capacity will be used. In addition, the gas supply system for the thrust bearing is now using nitrogen. The sonic velocity of nitrogen corresponds closely to the tip velocity of the shaft at 240,000 rpm. To avoid super-sonic flow in the thrust surfaces, helium will be used for future runs.

3.2.3 Starting Fluid

During this period of testing a new starting fluid has been used with excellent results. Freon 113 was substituted for the methyl alcohol used in the past. It was found that the electrical properties of alcohol were such that it adversely affected the probes and strain gages. Freon, since it is non-conducting, has no effect on the instrumentation.

3.3 Flexural Critical Speed Rig Test Results

The flexural critical speed test rig has previously been used to spin rotors supported on self-acting, air-lubricated foil bearings at speeds of approximately 250,000 rpm. Here the rotor is supported axially by two externally pressurized thrust bearings, and radially by two sets of three foil journal bearings. The shaft is rotated by means of gas impingement on the blading cut into the center of the shaft. Figure 17 shows two of the three rotors used with this test rig.

The two rotors shown are of stainless steel. The necked rotor has the same length and diameter as the solid rotor, except for the sections of smaller diameter. Another rotor made from magnesium was

constructed to the same dimensions as the necked steel rotor shown in Fig. 17. The measured first free-free, flexural critical speed of the magnesium rotor was 90,000 rpm, the necked stainless steel rotor speed was 100,000 rpm, and the solid stainless steel rotor speed was 336,000 rpm. The free-free frequency vibration was measured as the sound frequency emitted after striking the shafts, handing on silk threads, with a hammer.

Several attempts were made to accelerate these shafts through their respective flexural critical speeds. However, when the flexural critical speed of the shaft was approached the rotor orbit grew until there was contact with the capacitance motion-measuring probes. At this point, all of the shafts experienced violent low frequency oscillations. It was not possible to exceed this flexural critical speed with any of the shafts.

To accelerate the solid stainless steel rotor to its flexural critical speed (approximately 360,000 rpm) it was necessary to drive the turbine with helium gas. Air would not drive the rotor beyond 250,000 rpm.

Figure 18 shows relative orbital growth of the solid rotor. Figure 19 shows the orbital motion from 183,000 to 298,800 rpm. There was no noticeable change in orbit size over this range of rotational speeds, and at no point during the tests did the orbits exhibit half-frequency whirl instability. The fractional-frequency whirl at the flexural critical speed is shown in Fig. 20. This same fractional speed whirl is shown again at a lower shaft speed in Fig. 21. The frequency of this whirl is nearly constant; it is associated with the natural frequency of the mass of the rotor and the stiffness of the lubricating film and foil supports.

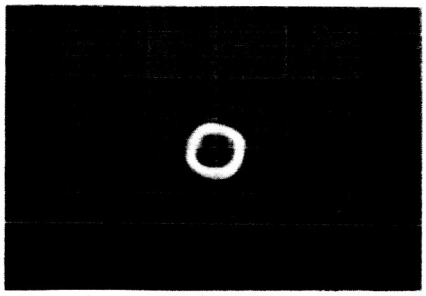

a) Rotational Speed: 120,000 rpm

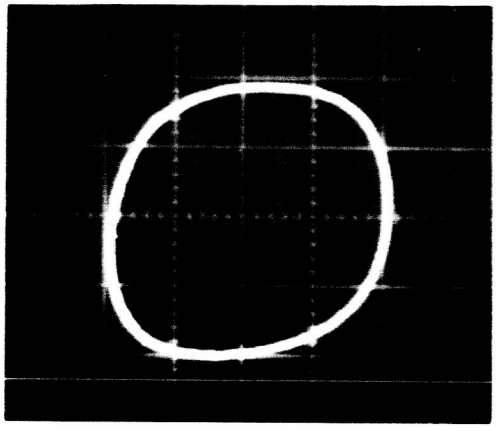

b) Rotational Speed: 347,000 rpm
(Approaching the Free-Free
Critical Speed of the Shaft)

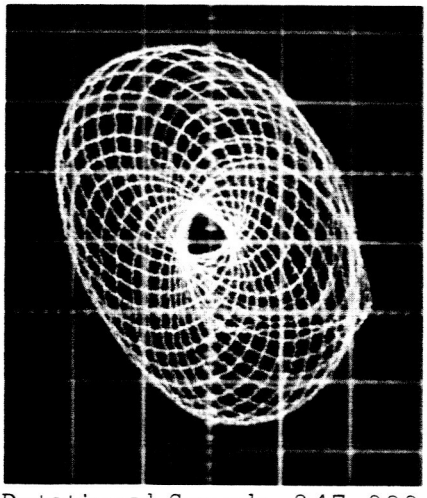

c) Rotational Speed: 347,000 rpm
(Near Shaft Free-Free Critical
Speed, Showing Subharmonic Motion)

Fig. 18 Lissajus Patterns Showing Orbits of Rotors
Supported on Foil Bearings

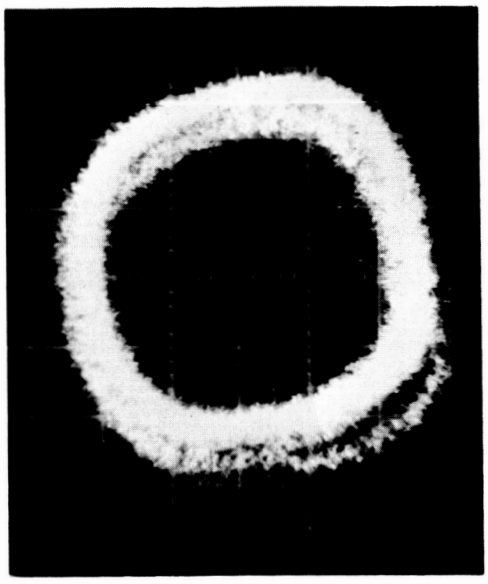

121,000 RPM
0.2 volt/cm

180,048 RPM
0.2 volt/cm

240,216 RPM
0.2 volt/cm

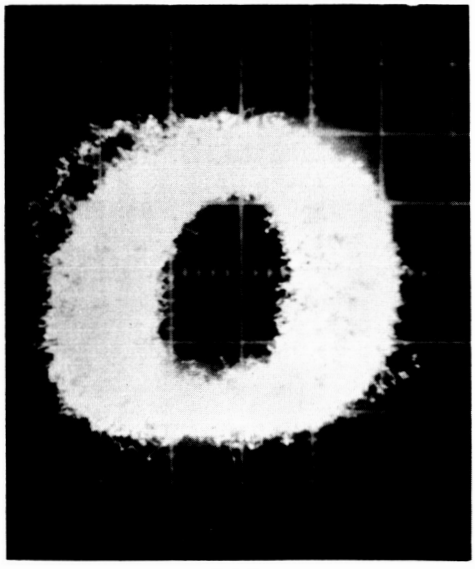

298,800 RPM
0.2 volt/cm

Fig. 19 Orbital Motion of 5/8 in. Dia. x 4.5 in. Shaft Supported on Helium Lubricated, Self-Acting Foil Bearings

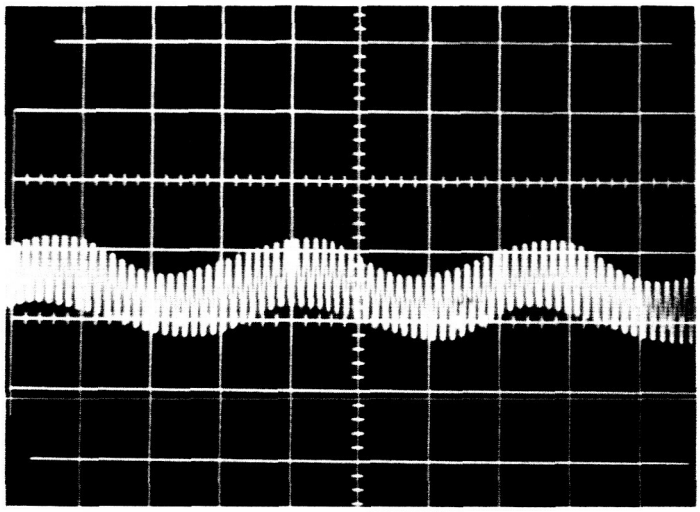

359,000 RPM
y = 5 volts/cm
x = 10 μ sec/cm (1/8)
Rotational Frequency = 5968 cps
Whirl Frequency ≈ 218 cps
Gas - Helium

Fig. 20 Shaft Motion at 359,000 rpm Showing Fractional Frequency and Synchronous Free-Free Critical Whirl

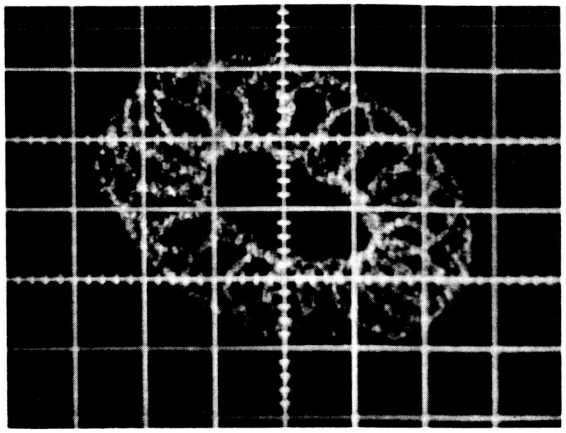

265,000 RPM
x, y = 0.5 volt/cm

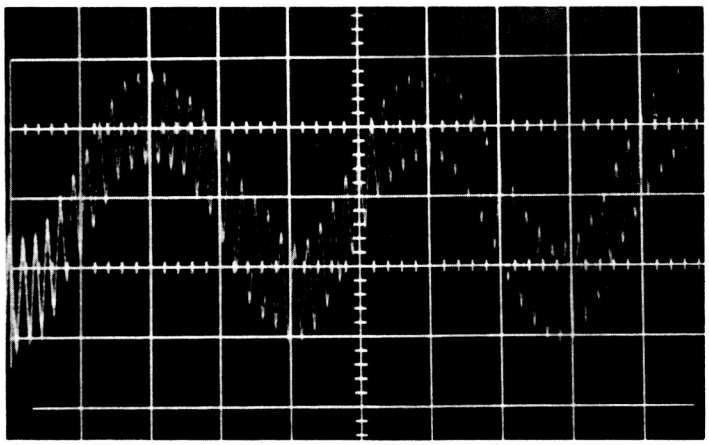

265,000 RPM
y = 0.5 volt/cm
x = 10 m sec/cm (1/8)

Rotational Frequency = 4408 CPS
Whirl Frequency ≈ 206 CPS
Lubricant - Helium

Fig. 21 Orbital Motion of Rotor at 265,000 rpm, a Fractional Frequency Critical Speed

Small frequency variations occurred which were apparently caused by foil tension changes. These changes were the result of the rubs and violent motions experienced at critical speeds and the foil tension may have varied throughout the test. Due to the manner in which the foils are mounted, the tension is a non linear function of deflection. It would seem reasonable therefore to expect a change in the fractional-frequency whirl as the shaft orbit varies. In Figs. 22 and 23, the fractional whirl is shown for lower shaft speeds.

Figure 24 shows the orbital motions of the solid steel rotor during and after a sharp impact to the test rig. The decay record has a predominant 170-cps component. Since the experimental whirl frequencies were from 154 to 218 cps, this data further supports the hypothesis that all of the fractional-frequency whirling motions were associated with the mass of the rotor and the low positional stiffness of the self-acting foil bearings used to support the rotor.

3.4 High Speed Test Rig-Test Results *

Figures 25 through 27 are photographs of orbits and shaft motions taken from the high-speed rig. During a given run, the foil tension and wrap angle were held constant and speed varied. Foil tension was adjusted while the shaft was rotating at approximately 60,000 rpm. There was no noticeable change in foil tension as speed was increased. Foil tensions of 2.2, 3.1, and 4.0 lbs/in. were used. Wrap angles, θ were 150° and 210°. With 150° wrap, it was possible to make runs with all foil tensions. With 210° wrap however, it was very difficult to start at 3.1 lbs/in. and starts could not be made at all at 4.0 lbs/in. tension. Foil material used throughout this phase of testing was 0.001 in. Havar. In future testing an effort will be made to reduce the high starting

* This section was done by A. L. Huckabay

torques experienced in some of the tests.

The outputs of the capacitance probes, the dynamometer and rotational speed were all recorded on magnetic tape. The tape speed was always 60 in./sec when recording. This speed may then be reduced to 30, 15, or 7 1/2 ips when the data is being reproduced.

Figure 25 shows shaft orbits at two speeds with air lubrication and whirl frequencies at high speed with helium. The magnitude of the excursions may be found from the vertical scale. At 240,000 rpm the maximum radial excursion is approximately 0.001 in. Figure 26 shows orbital motions with the whirl frequencies displayed alongside for comparison. As in Fig. 25, the predominant whirl frequency is approximately 26 cps. This frequency is associated with the natural frequency of the rotor mass, film stiffness, and foil support structure. Figure 27 is a comparison of the impact response at various wrap angles and foil tensions. As would be expected, as foil tension and wrapping increase so does the frequency at which the system whirls after impact. The orbit shown in Fig. 27 is typical of those for all conditions immediately after impact.

Figures 28 and 29 are comparisons of theoretical and experimental viscous torques. In all cases, measured torques were higher than predicted by theoretical analysis. The theoretical torque equation is based on laminar flow in all regions of the foil bearings. As can be seen from Fig. 29, this foil drag is Reynolds number dependent. In bearing configurations tested, the entrance and exit regions were turbulent. However, the Taylor critical Reynolds number was not

exceeded in the constant gap region. The film thickness was calculated under the laminar flow assumption of reference 4. From this reference it can be shown that over the angle of wrap required to build the film pressure up to T/R, the film thickness undergoes a ten to one reduction, yielding a thirty fold increase in Reynolds number at the entrance. This is sufficient to cause turbulent flow. Under these conditions the film thickness will be reduced throughout the wrap and the foil drag will increase due to this reduced gap and turbulent flow.

In addition, the Mach number at 180,000 rpm is 0.70. The results shown in Figs. 28 and 29 probably reflect the difference between laminar foil drag and turbulent foil drag including compressibility effects.

194,000 RPM
x, y = 0.2 volt/cm

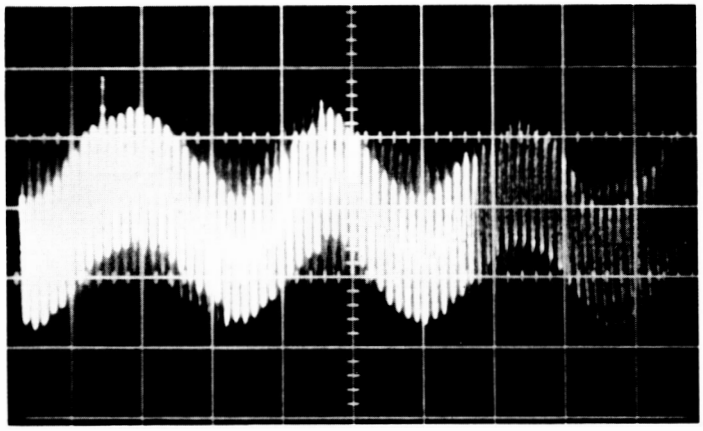

194,000 RPM
y = 15 volt/cm
x = 10 μ sec/cm (1/4)

Rotational Frequency = 3232 cps
Whirl Frequency ≈ 154 cps
Lubricant: Helium

Fig. 22 Shaft Orbital Motion at 194,000 rpm Fractional Frequency Whirl Critical Speed

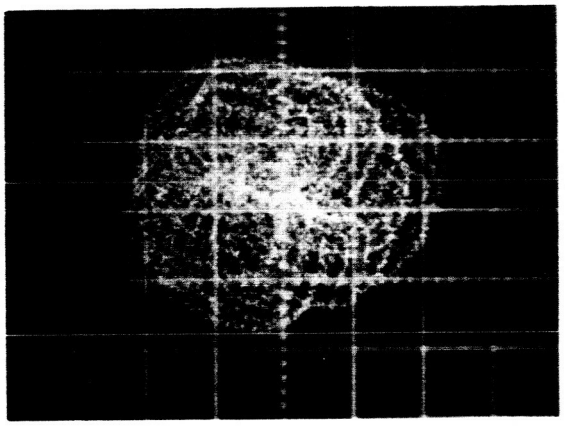

178,000 RPM
x, y = 0.2 volt/cm

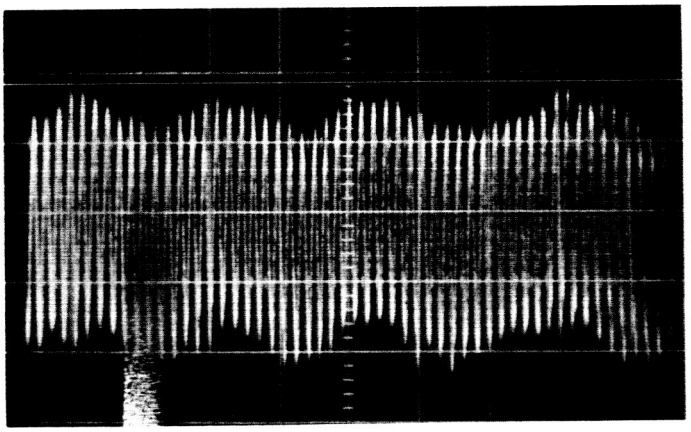

178,000 RPM
y = 0.2 volt/cm
x = 10 m sec/cm

Rotational Frequency = 2129 CPS
Whirl Frequency ≈ 177 CPS
Lubricant - Air

Fig. 23 Shaft Orbital Motion at 178,000 rpm, a Fractional Frequency Whirl Critical Speed

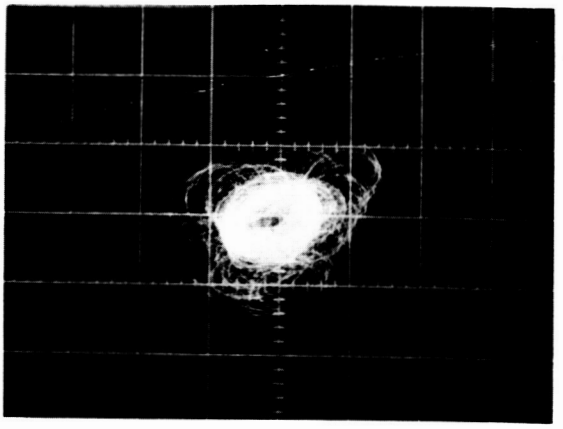

127,000 RPM
x, y = 0.5 volt/cm

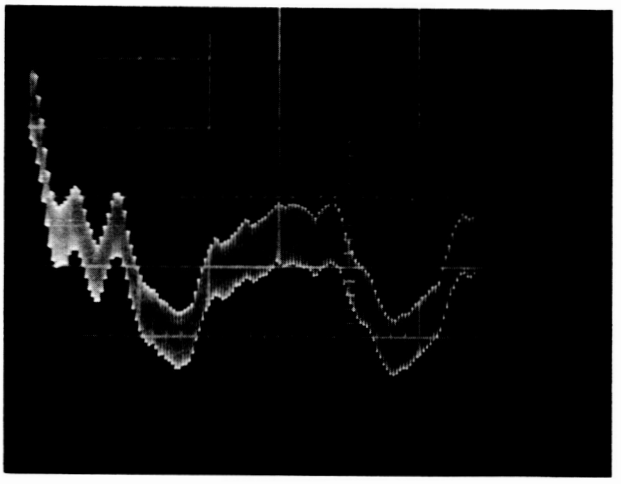

127,000 RPM
y = 0.5 volt/cm
x = 10 m sec/cm

Rotational Frequency = 2129 CPS
Whirl Frequency ≈ 170 CPS
Lubricant - Air

Fig. 24 Shaft Orbital Motion at 127,000 rpm, After Impact

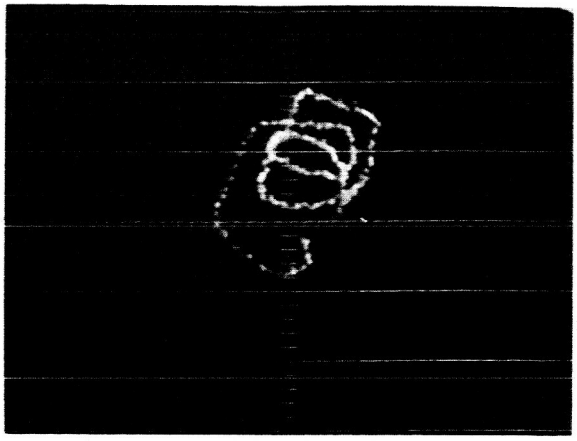

34,000 rpm
x, y = 50 microin/cm
Gas - Air

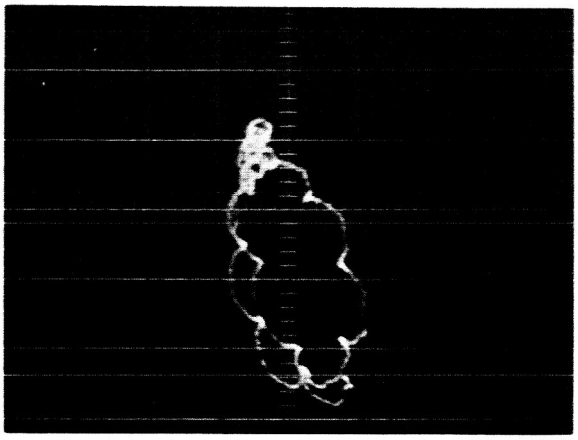

97,000 rpm
x, y = 250 microin/cm
Gas - Air

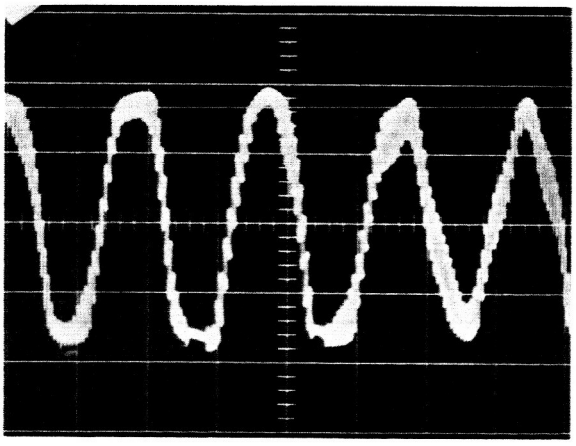

240,000 rpm
x = 20 msec/cm
y = 500 microin/cm
Whirl Frequency = 27 cps
Turbine On
Gas - Helium

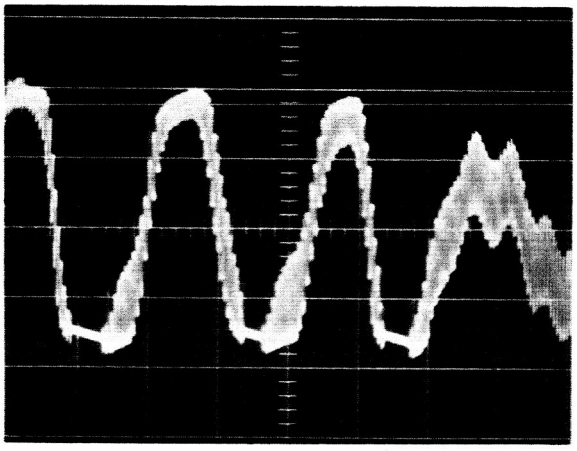

240,000 rpm
x = 20 msec/cm
y = 500 microin/cm
Whirl Frequency = 27 cps
Turbine Off
Gas - Helium

Fig. 25 Orbital Motion of 1 in. Dia. Shaft Supported on Air and Helium Lubricated Self-Acting Foil Bearings. Wrap Angle = 210°, Foil Tension = 2.20 lb/in.

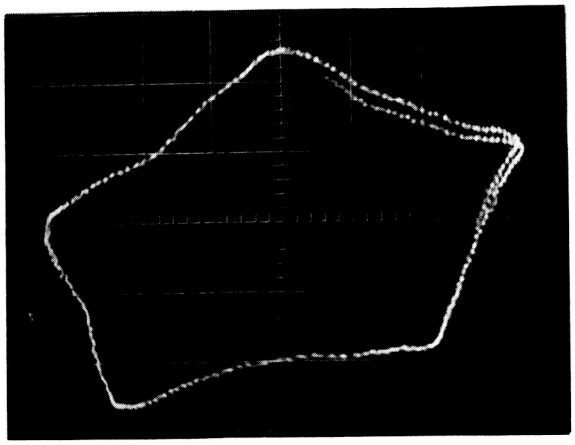

25,600 rpm
x, y = 100 microin/cm

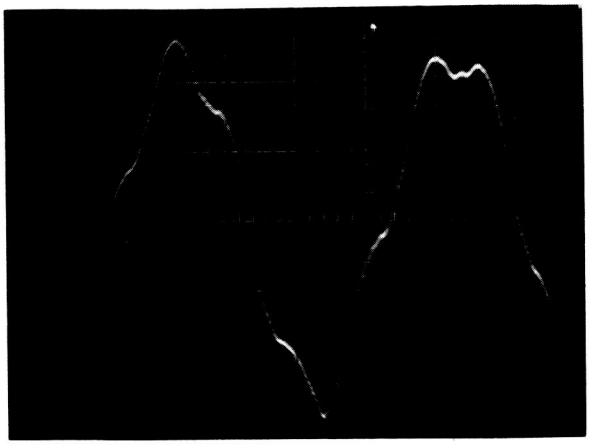

26,200 rpm
x = 10 msec/cm y = 100 microin/cm
Whirl Frequency = 27 cps

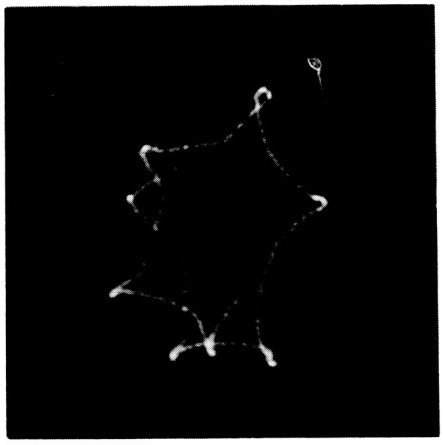

71,500 rpm
x, y = 100 microin/cm

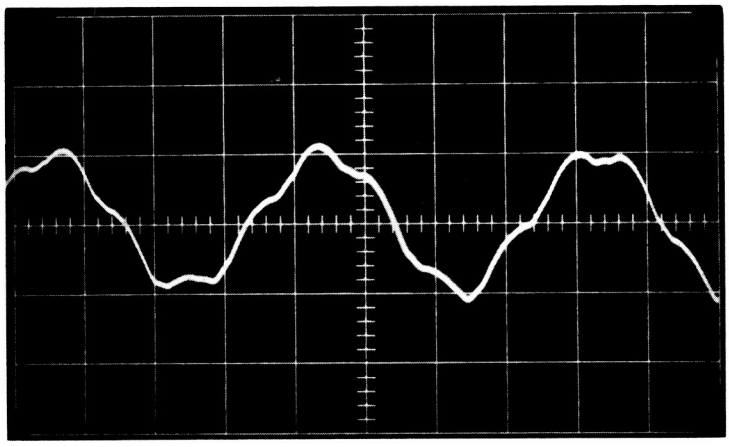

71,500 rpm
x = 10 msec/cm y = 250 microin/cm
Whirl Frequency = 26 cps

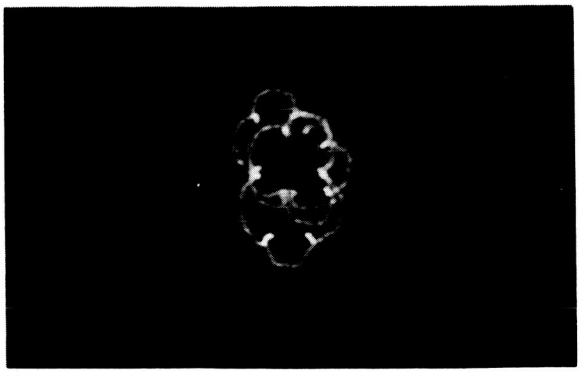

97,000 rpm
x, y = 250 microin/cm

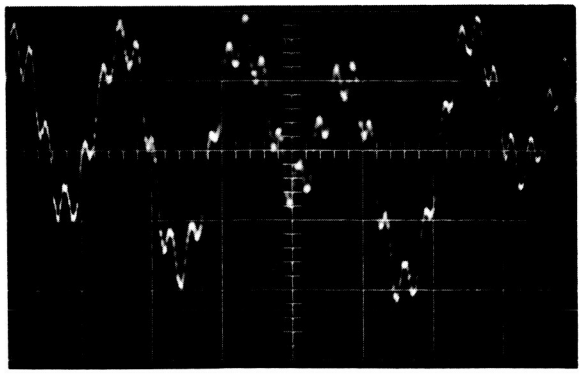

97,000 rpm
x = 10 msec/cm y = 100 microin/cm
Whirl Frequency = 60 cps

Fig. 26 Orbital Motion of 1 in. Dia. Shaft Supported on Air Lubricated Self-Acting Foil Bearings. Wrap Angle = 210°, Foil Tension = 2.20 lb/in.

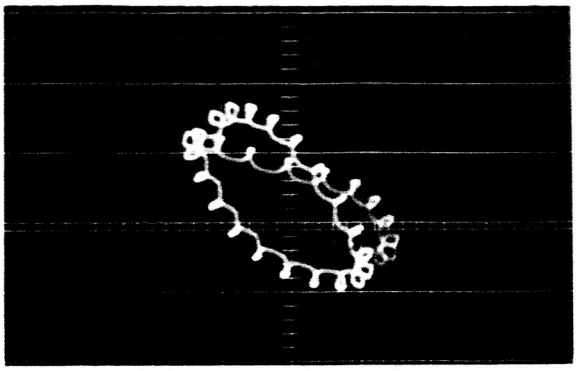

71,600 rpm
x, y = 250 microin/cm
150° wrap
2.2 lb/in tension

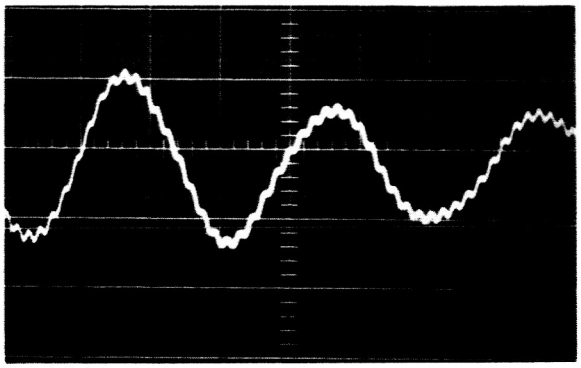

71,600 rpm
x = 20 msec/cm y = 500 microin/cm
Whirl Frequency = 17 cps
150° wrap, 2.2 lb/in tension

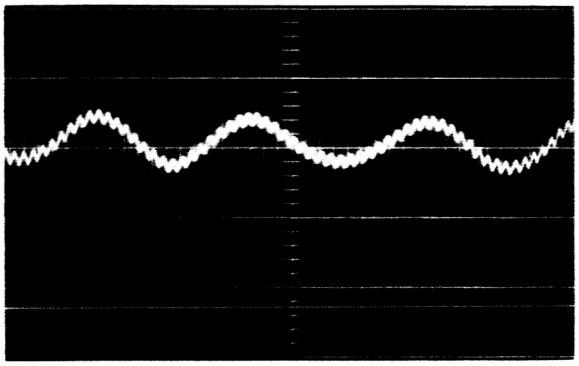

89,500 rpm
x = 20 msec/cm y = 500 microin/cm
Whirl Frequency = 21 cps
150° wrap, 3.1 lb/in tension

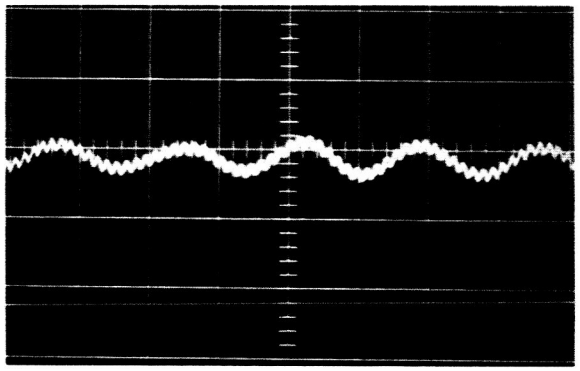

89,300 rpm
x = 20 msec/cm y = 500 microin/cm
Whirl Frequency = 29 cps
150° wrap, 4.0 lb/in tension

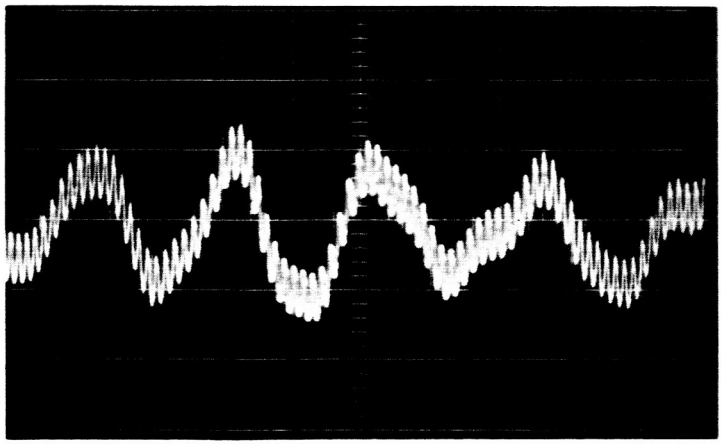

94,000 rpm
x = 20 msec/cm y = 500 microin/cm
Whirl Frequency = 23 cps
210° wrap, 2.2 lb/in. tension

Fig. 27 Impact Response of 1 in. Dia. Shaft, Varying as a Function of Foil Wrap Angle and Foil Tension.

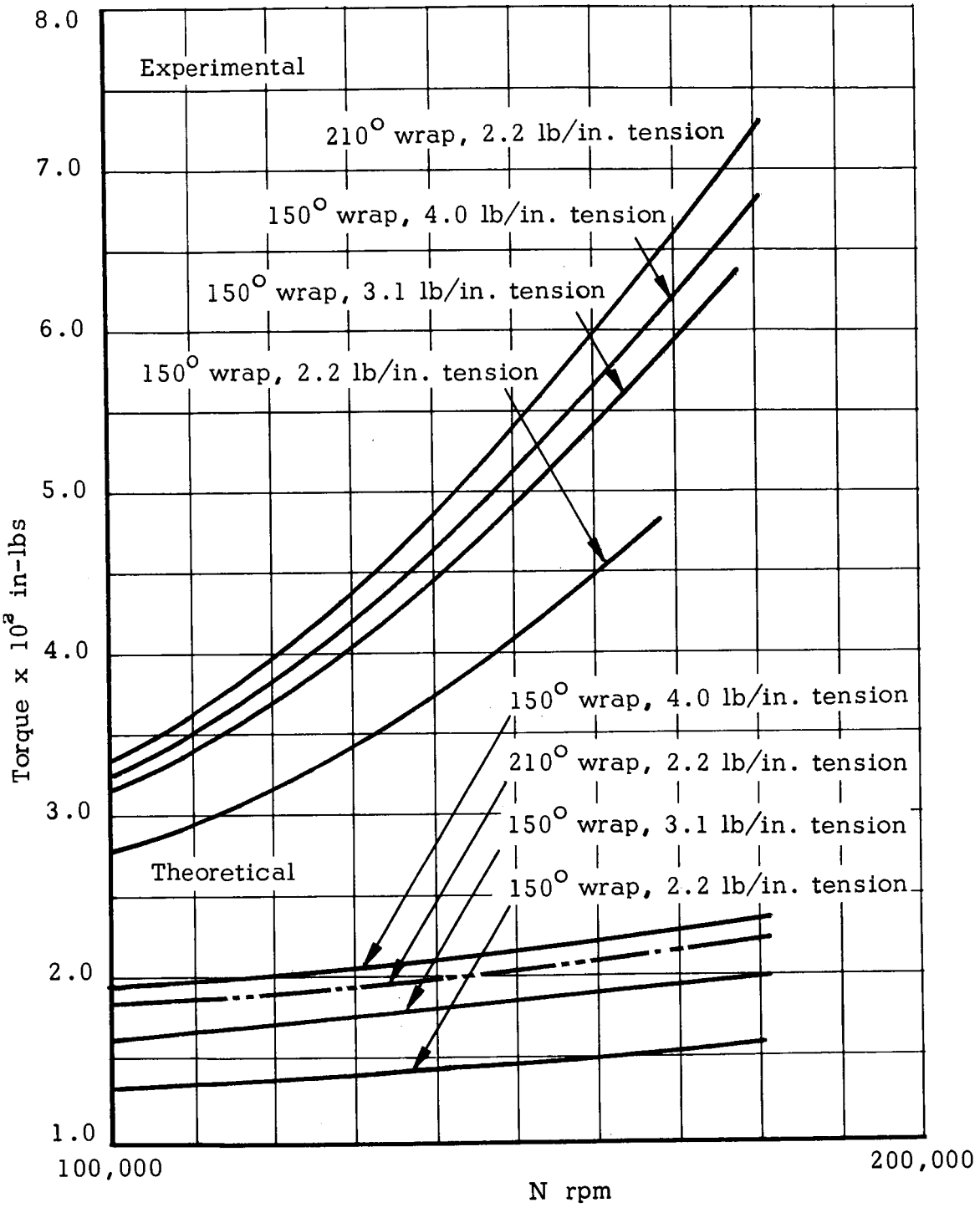

Fig. 28 Comparison of Experimental and Theoretical Foil Bearing Drag Results

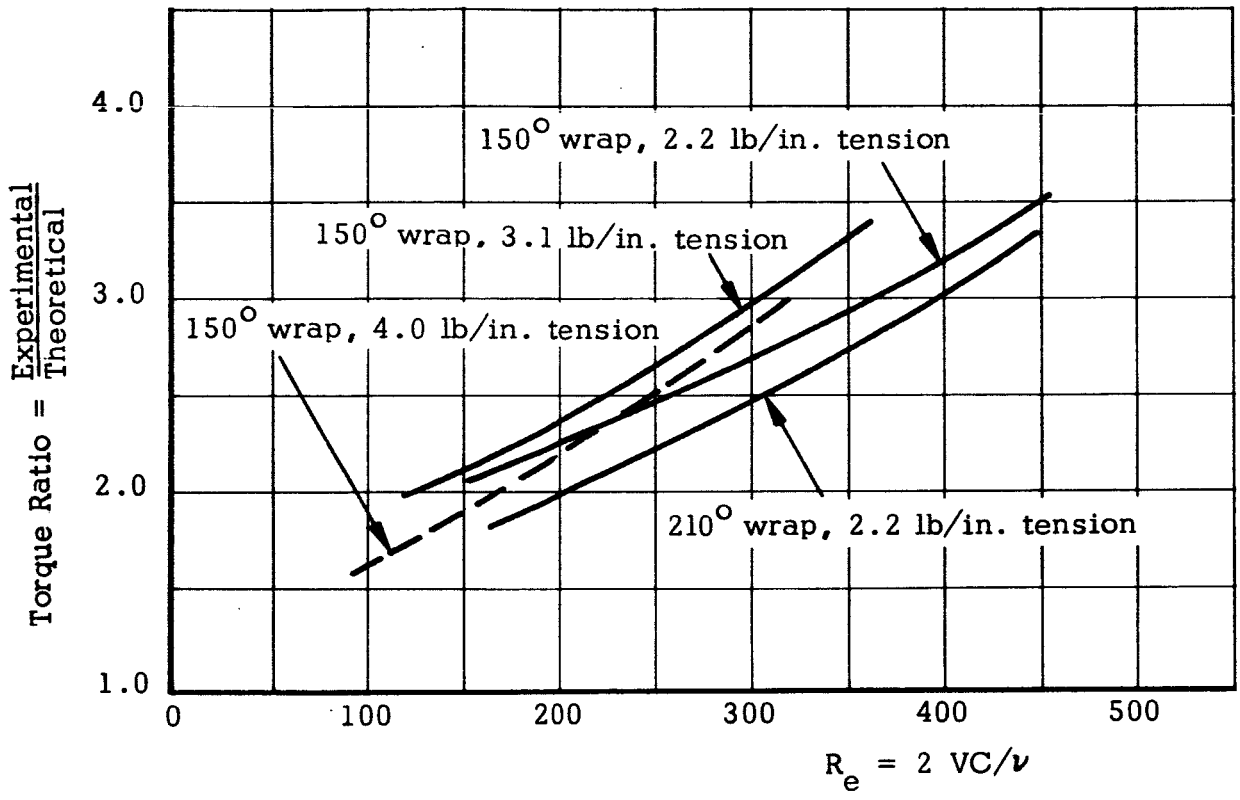

Fig. 29 Comparison of Experimental and Theoretical Foil Bearing Drag Results as a Function of Reynolds Number

APPENDIX 1

The Support of a Rotor on Self-Acting Gas Lubricated Foil Journal Bearings

The self-acting gas lubricated foil journal bearing can be used to support a high-speed rotor. This type of journal bearing has been shown to be free from the self-excited half-frequency whirl instability that limits the speed of conventional gas lubricated bearings. The only limitation to rotational speed of a rotor supported by a foil journal bearing is the occurrence of the first flexural critical speed of the rotor.

The foil journal bearing is free from self-excited half-frequency whirl because of the flexibility of the foils. However, this flexibility coupled with the elasticity of the supporting foils often results in a rotor support with a relatively low radial or positional stiffness. Due to this low positional stiffness there are low frequency, rigid body, critical speeds through which the rotor bearing system must be accelerated. These critical speeds are associated with the mass, length and polar moment of inertia of the rotor and the location and geometry of the supporting foils. The occurrence of these critical speeds and the low positional stiffness of the foil journal bearing often precludes its use in many practical applications.

The object of this analysis is to present the support characteristics of self-acting, gas-lubricated foil journal bearings in terms of the physical quantities involved. With this information, the designer can then manipulate these several parameters to obtain a self-acting foil journal bearing that is compatible with the particular rotor support application.

Figure A-1 shows a schematic of a self-acting foil journal bearing used to support a rotating shaft. Figure A-2 shows the equivalent mass- spring representation of the foil bearing rotor support. In this case, the rotor is centered within the supporting structure by three foils each of which is wrapped about the rotor with an angle θ. These foils have a tension of T lbs. per unit width of foil. When the shaft rotates with tangential velocity U, the surrounding gas lubricant is brought into each of the foil bearings and the lubricating film thickness can be expressed as[4]

$$\frac{h}{R}\left(\frac{T}{6\mu U}\right)^{2/3} = .643 \qquad \text{(A-1)}$$

Equation (A-1) gives the lubricating film thickness in the constant gap region of the foil bearing. The clearances at the inlet and exit regions differ from that in a constant gap region; however, Baumeister[5] has shown that the extent of these regions is approximately 20 times the lubricating film thickness, which is usually an insignificant distance compared to the bearing length. For this preliminary analysis, the entrance and exit regions will be ignored.

The relationships of foil tension, rotational speed, and air film thickness for a self-acting foil journal bearing operated in a gas with a viscosity of 0.26×10^{-8} reyns is shown in Fig. A-3. Note that the air film thickness is not a function of the wrap angle of the foil. The radial centering force F, however, decreases with the decreasing wrap angle,

$$F = 2T \sin\frac{\theta}{2} \qquad \text{(A-2)}$$

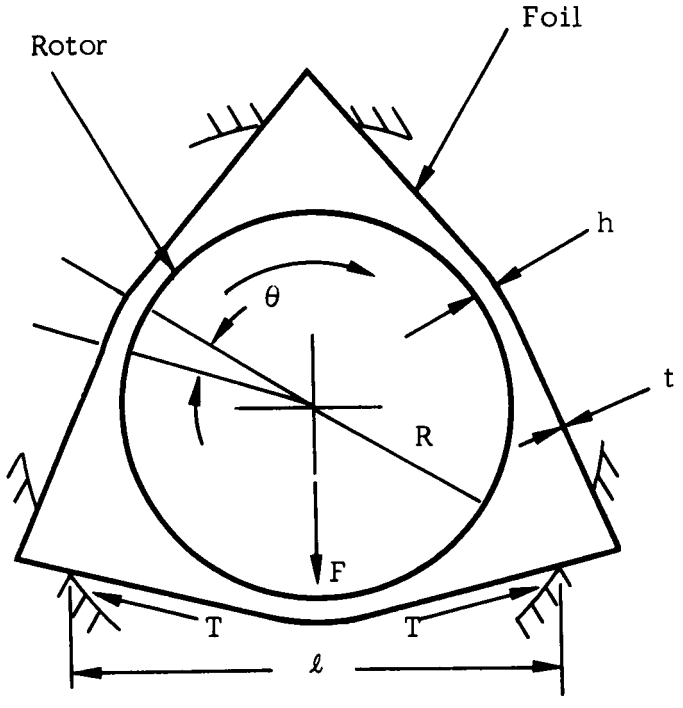

Fig. A.1 Schematic Representation of a Rotor Supported on Self Acting Foil Journal Bearings

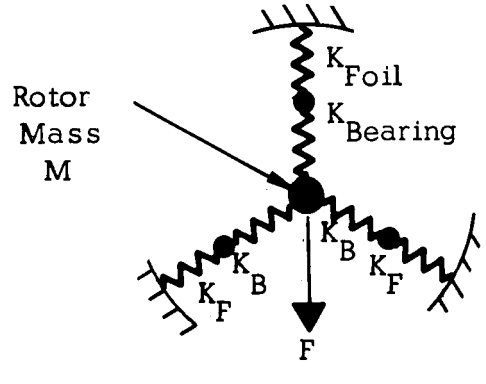

Fig. A.2 Mass-Spring Equivalent of Foil Bearing Rotor Support

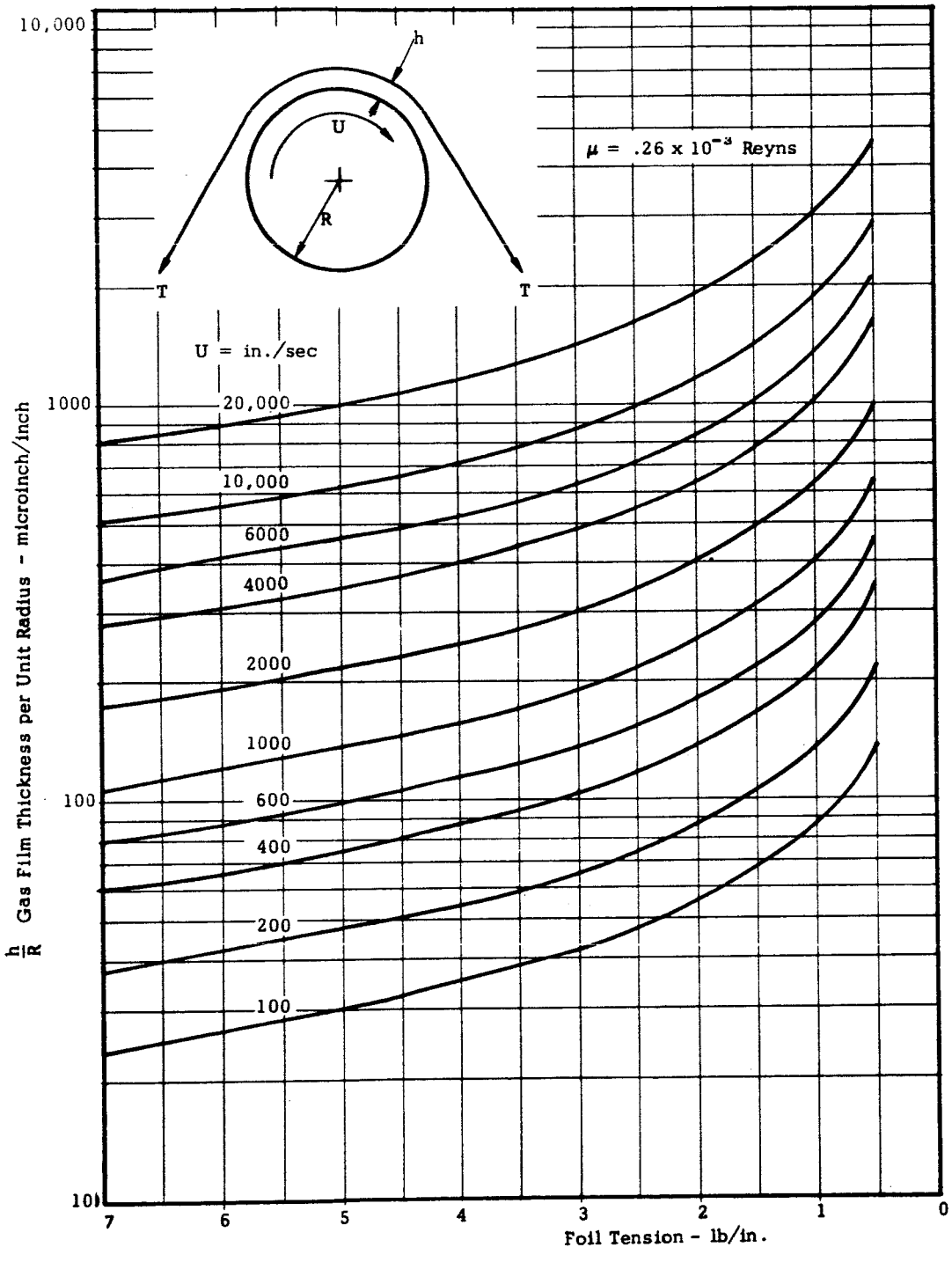

Fig. A-3 Characteristics of a Self-Acting Gas Lubricated Foil Journal Bearing

This equation is shown in Fig. A-4. The radial stiffness $\left(\frac{dF}{dh}\right)$ of a lubricating film of a single self-acting foil journal bearing can be obtained by substitution of Eq. (A-1) into Eq. (A-2) and differentiating with respect to h,

$$K_B = \frac{dF}{dh} = -3 \times .643^{3/2} (6\mu U) \frac{R^{3/2}}{h^{5/2}} \sin\frac{\theta}{2} \qquad \text{(A-3)}$$

$$\mu = .26 \times 10^{-8} \text{ reyn}$$

$$\left(\frac{dF}{dh} \times \frac{1}{U}\right) = -3.48 \frac{R^{3/2}}{h^{5/2}} \sin\frac{\theta}{2} \times 10^{7} \qquad \text{(A-4)}$$

Equation (A-4) with $\theta = \pi$ is shown in Fig. A-5 as a function of radius R. The relationship between the stiffness per unit speed, speed, and radial stiffness for a 180° wrap foil are shown in Fig. A-6

The gas film is formed between the shaft and the foil and the foil is connected at its extremities to the supporting structure. In general, a foil that is sufficiently flexible to conform to the self-acting pressure distribution within the lubricating film over the shaft will be elastic and extensible. The support stiffness of this elastic foil is

$$K_F = \frac{2tE}{\ell} \sin^2\theta \qquad \text{(A-5)}$$

The overall radial stiffness of each portion of the foil journal bearing can be obtained by treating the gas film and the foil stiffness as two springs connected in series as represented in Fig. A-2.

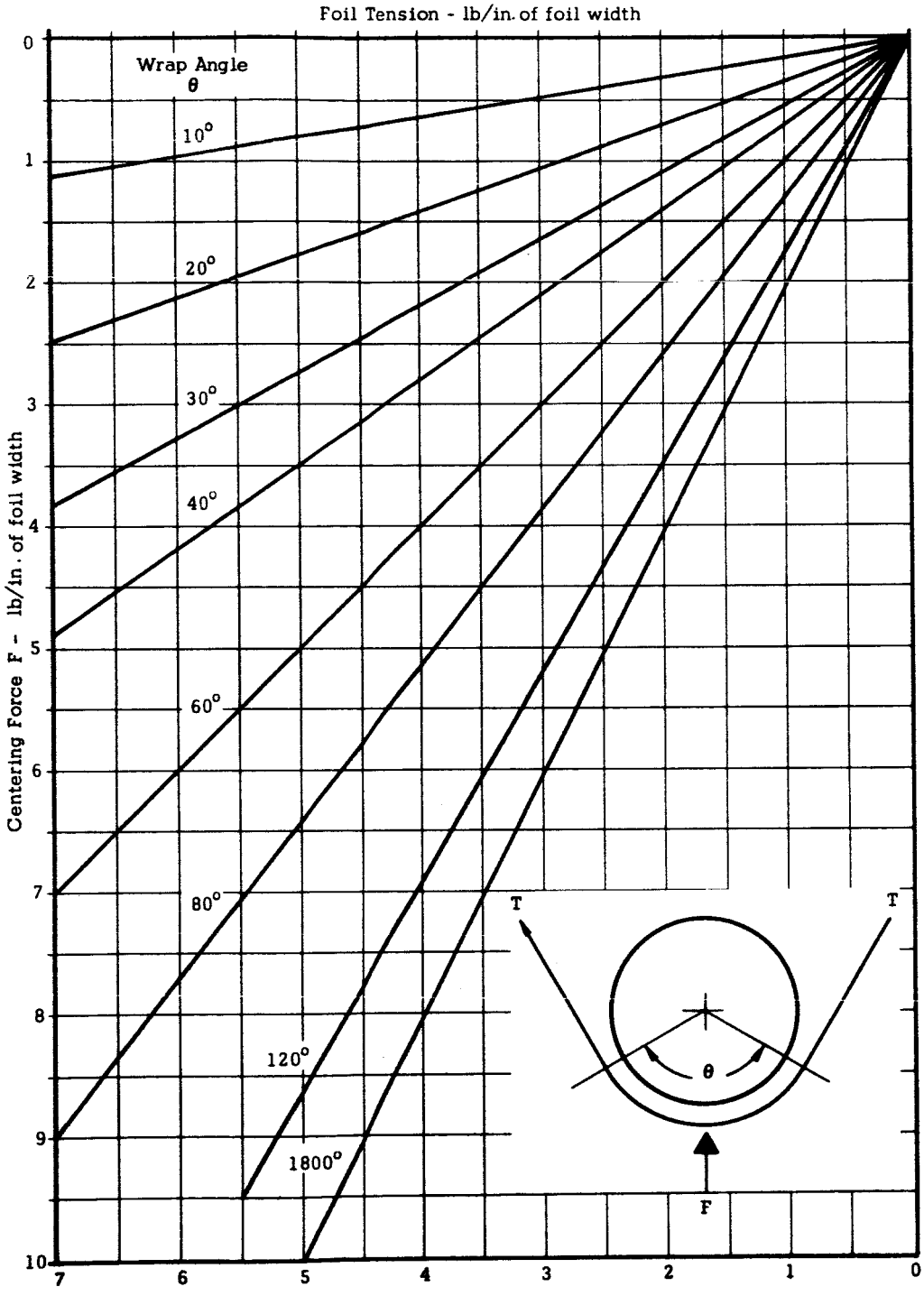

Fig. A-4 Centering Force of a Foil Journal Bearing as a Function of Wrap Angle and Foil Tension

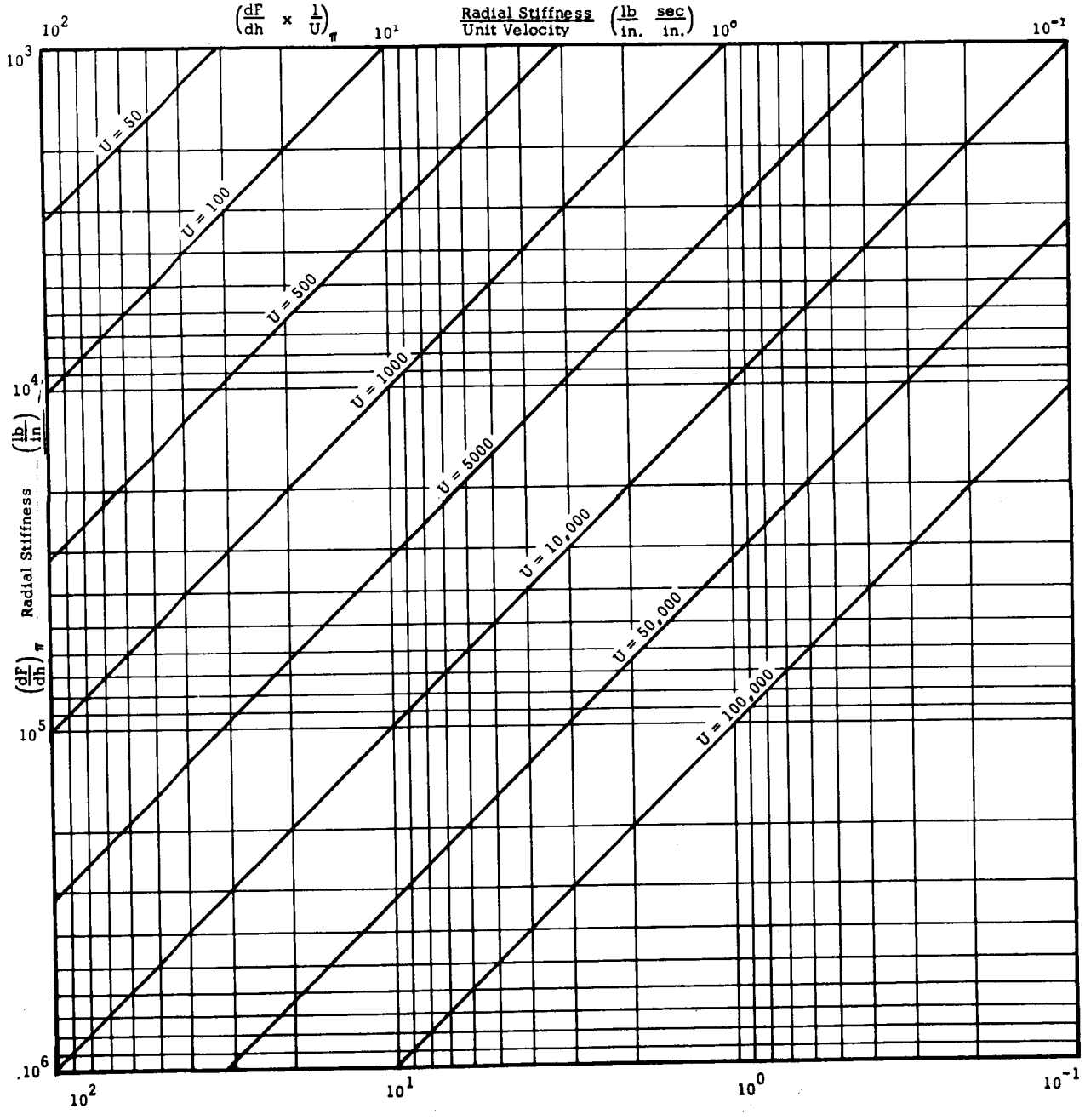

Fig. A-5 Radial Stiffness per Unit Velocity of Self-Acting Foil Journal Bearings

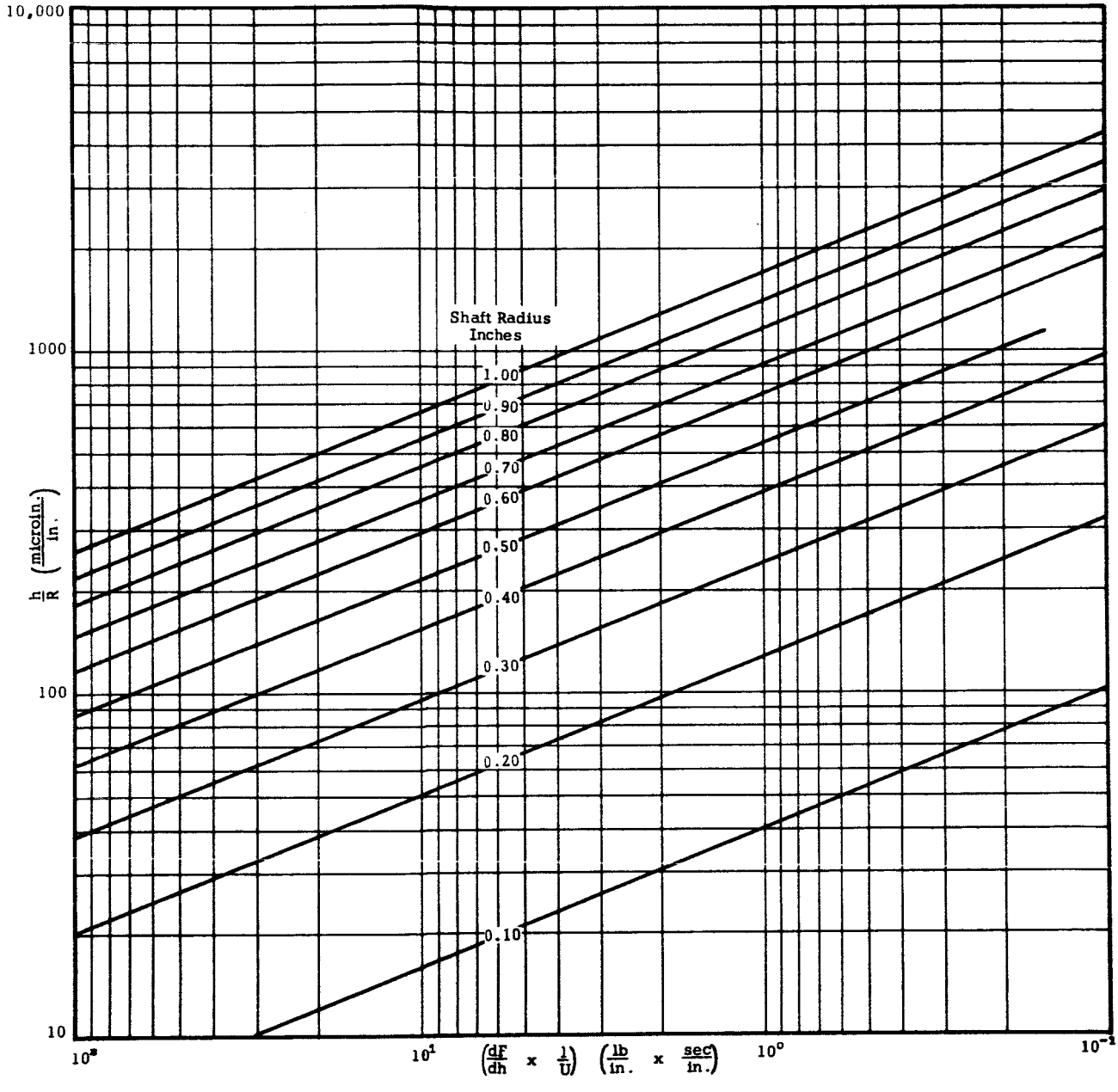

Fig. A-6 Radial Stiffness of Self-Acting Foil Journal Bearings

$$K = \frac{K_F K_B}{K_F + K_B} \qquad \text{(A-6)}$$

The total radial stiffness of a particular foil bearing rotor support can be obtained from Eq. (A-6) multiplied by one-half the number of individual foils in the bearing.

The viscous frictional force exerted on the foil over the constant gap region per unit width of each foil journal bearing can be expressed as in reference 6 .

$$f = \mu U \frac{R}{h} \Theta \qquad \text{(A-7)}$$

With a given set of rotor bearing conditions, ie. U, R, μ, θ, T, t, E, l, these equations and graphs can be used to obtain the radial stiffness and frictional drag of a foil bearing rotor support system. The information, however, is not sufficient to describe these parameters over a wide range of speeds. This limitation is imposed by the conflicting requirements of Eqs. (A-1) and (A-5). Equation (A-1) requires an increasing lubricating film thickness with increasing rotational speed, but this increased film thickness can only be obtained through stretching of the supporting foil, which increases the foil tension. The support characteristics of the self-acting foil journal bearing, therefore, requires the simultaneous solutions of Eqs. (A-1) and (A-5) with particular geometry of foils and support under consideration. This solution will be presented in the next quarterly progress report.

APPENDIX II

On the Attitude Angle of Foil Bearings*

1. INTRODUCTION

The stability of a bearing is closely tied to the attitude angle (the measured angle from the load vector to the displacement vector, positive when in the direction of rotation and negative when not). It is of interest, therefore, to investigate this angle for foil bearings. For brevity, let the direction of the load be termed vertical and the direction of its normal horizontal. The investigation will be restricted to steady state conditions.

The horizontal component of the load depends on the foil-fluid system and on the horizontal mobility of the supports of the foil. The vertical component of the displacement depends on the foil-fluid system, on the vertical mobility of the foil through its supports (i.e., the mechanism, if any, for collecting slack), and on the extension of the foil.

In reference 4 it is shown (see Fig. A-7) that $h_e = r_o H_e \left(\frac{6\mu U}{T}\right)^{2/3} < 0$; $h_i = r_o H_i \left(\frac{6\mu U}{T}\right)^{2/3}$; $h^* = r_o H^* \left(\frac{6\mu U}{T}\right)^{2/3}$ where H_e, H_i, and H are constants given in reference 4. If no slack is collected, the length of the foil between the supports ℓ is related to its initial length ℓ_o by $\ell = \ell_o \left(1 + \frac{T}{Et}\right)$. When the load on the shaft is changed while steady state conditions prevail, the change in tension modifies h_i, h_e, h^* as well as the length of the foil. The combination

*This section was done by Abe Eshel.

of these factors, geometrical considerations, and the mobility of the supports, determines the equilibrium locus of the center of the shaft under load. In the following some specific cases are considered.

2. Single Foil System with 180° Wrap

Case 1: Load parallel to asymptotes; foil free to move normal to the asymptotes

In this case the static response of the shaft to load is motion parallel to the asymptotes (vertical). Thus, the attitude angle is zero.

Case 2: Load parallel to asymptotes; centerline of foil bearing* remains fixed

In this case the distance of each foil from the centerline is $r_o + \frac{h_i + h_e}{2}$. The distance of the center of the shaft from the center line is $\delta = \frac{h_i - h_e}{2}$.

The horizontal distance δ may be evaluated also in a different manner. The overall equilibrium of the fluid system requires

$$W = 2T \qquad \text{(balance of forces)} \tag{A-1}$$

$$W \cdot \delta = \oint (\tau_s - \tau_r) r_o^2 \, d\theta \qquad \text{(balance of moments)} \tag{A-2}$$

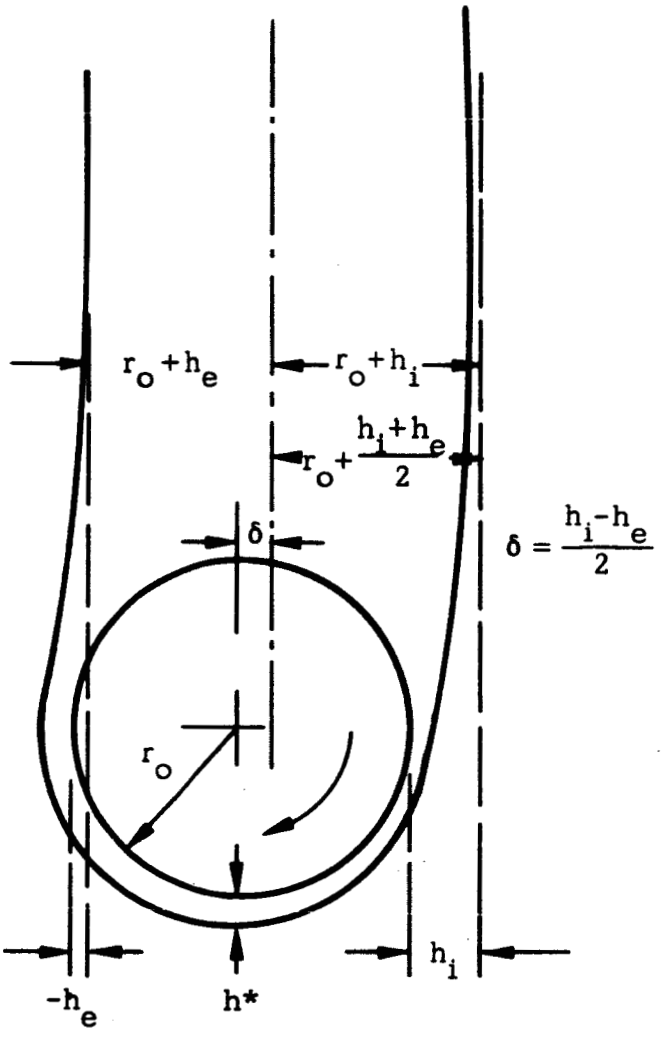

Fig. A-7 Single Foil System with 180° Wrap Angle

where τ_s and τ_f are the shears of the shaft and the foil on the fluid respectively. According to the Reynolds approximation:

$$\tau_s - \tau_f = \left(\frac{\partial p}{\partial s}\frac{h}{2} - \mu\frac{v}{h}\right) + \left(\frac{\partial p}{\partial s}\frac{h}{2} + \mu\frac{v}{h}\right) = \frac{\partial p}{\partial s}h \qquad \text{(A-3)}$$

Substituting in Eq. (A-3)

$$\frac{dp}{ds} = 6\mu v\,\frac{h - h^*}{h^3} \qquad \text{(A-4)}$$

$$h = r_0 H \left(\frac{6\mu v}{T}\right)^{2/3} \qquad \text{(A-5)}$$

$$ds = r_0 d\xi \left(\frac{6\mu v}{T}\right)^{1/3} \qquad \text{(A-6)}$$

$$p - p_a = \frac{T}{R} = T\left(\frac{1}{r_0} - \frac{1}{r_0^2}\frac{d^2h}{d\theta^2}\right) \qquad \text{(A-7)}$$

one finds from Eq. (A-2).

$$W\cdot\delta = -\frac{T}{r_0}\oint \frac{d^3h}{d\theta^3}\,h\,d\theta = -T r_0\left(\frac{6\mu v}{T}\right)^{2/3}\left[H\frac{d^2H}{d\xi^2}\right]_{-\infty}^{\infty}$$

$$+\frac{T r_0}{2}\left(\frac{6\mu v}{T}\right)^{2/3}\left[\left(\frac{dH}{d\xi}\right)^2\right]_{-\infty}^{\infty}$$

*The centerline of the foil bearing is defined here as the line of action of the resultant of the two foil tensions.

With the boundary conditions[4],

$$H(\infty) \sim \frac{\xi}{2} + H_a$$
$$H'(\infty) \sim \xi \qquad \text{(A-9)}$$
$$H'' \sim 1$$

hence

$$W \cdot \delta = (2\tau)\, r_0 \left(\frac{6\mu v}{\tau}\right)^{2/3} \frac{H_i - H_e}{2} = (2\tau)\, \frac{h_i - h_e}{2} \qquad \text{(A-10)}$$

or: $$\delta = \frac{h_i - h_e}{2}$$

It is thus found that a moment $W \cdot \delta$, independent of wrap angle, acts on the fluid system. In order to find the attitude angle, it is necessary to find the vertical displacement. For the inextensible foil,

$$2y + (r_0 + h^*)\pi = l_0$$
$$\delta y = -\frac{\pi}{2}\delta h^* \qquad \text{(A-11)}$$
$$tg|\phi| = \frac{\delta h_i - \delta h_e}{2\left(\frac{\pi}{2}\delta h^*\right)} = \frac{H_i - H_e}{\pi H^*} = \frac{2.820 + 0.646}{\pi} \cong \frac{2\sqrt{3}}{\pi}$$

$$\phi = -47.8^\circ \qquad \text{(A-12)}$$

3. Single Foil System With Θ-Wrap

Case 1: Foil supports free to move perpendicularly to the asymptotes

As in the 180° wrap case, the angle between the displacement vector and the load is zero.

Case 2: The centerline of the foil is fixed

Since the value of $\oint r_o^2 (\tau_s - \tau_f)\, ds$ is independent of Θ, it follows that (see Fig. A-8 for notation)

$$W \cdot \delta = T r_0 \left(\frac{6\mu U}{T}\right)^{2/3} (H_i - H_e) \qquad \text{(A-13)}$$

But

$$W = 2T \sin\frac{\Theta}{2} \qquad \text{(A-14)}$$

hence

$$\delta = \frac{r_0 \left(\frac{6\mu U}{T}\right)^{2/3} (H_i - H_e)}{2 \sin\frac{\Theta}{2}} \qquad \text{(A-15)}$$

$$y = x \sin\frac{\Theta}{2} - (r_0 + h^*) \cos\frac{\Theta}{2} \qquad \text{(A-16)}$$

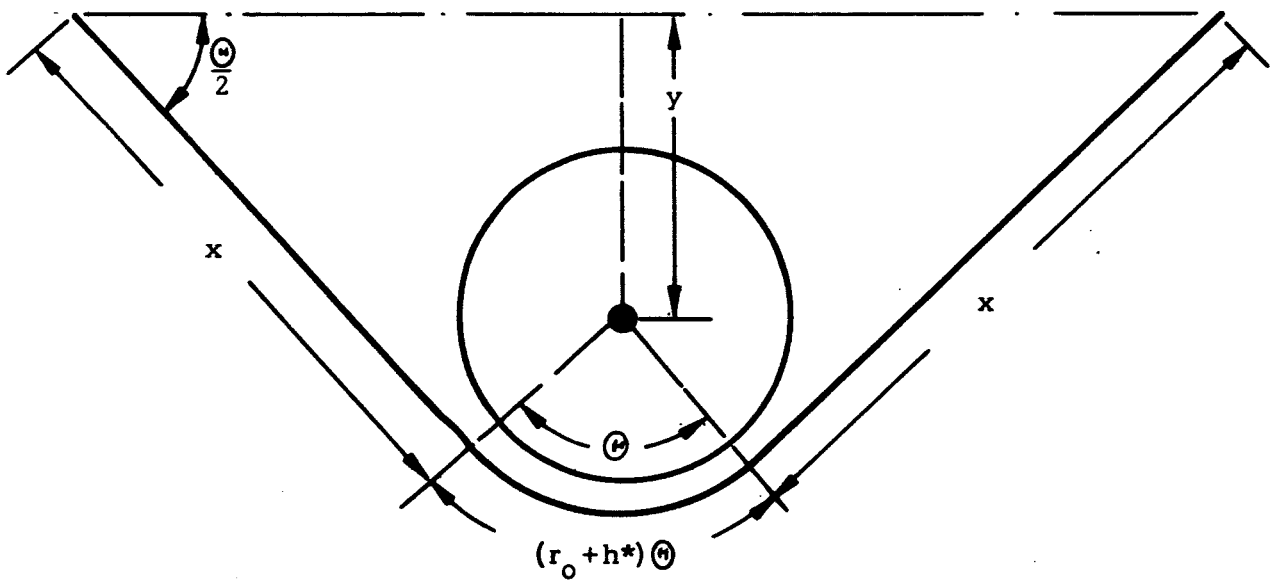

Fig. A-8 Single Foil System with Θ Wrap

$$x + (r_o + h^*)\frac{\Theta}{2} = \frac{l_o}{2} \tag{A-17}$$

$$\delta y = -\delta h^* \left(\frac{\Theta}{2}\sin\frac{\Theta}{2} + \cos\frac{\Theta}{2}\right) \tag{A-18}$$

$$tg|\phi| = \frac{H_i - H_e}{2H^*\sin\frac{\Theta}{2}\left(\frac{\Theta}{2}\sin\frac{\Theta}{2} + \cos\frac{\Theta}{2}\right)} \cong \frac{\sqrt{3}}{\sin\frac{\Theta}{2}\left(\frac{\Theta}{2}\sin\frac{\Theta}{2} + \cos\frac{\Theta}{2}\right)} \tag{A-19}$$

4. Three Foil System with Θ Wrap

Consider first a stationary, frictionless, three-foil system, each of wrap angle Θ. Each foil is assumed to be initially under tension T_o, but the shaft is not loaded. Each foil exerts a resultant reaction of magnitude $2T_o \sin\frac{\Theta}{2}$ passing through the center of the shaft.

Let the origin of the system of coordinates be located at the center of the shaft in the above condition. Suppose that rotation at an

angular velocity ω starts now, while the shaft is still load-free. The load on each foil by virtue of the initial tension is $P_o = 2T_o \sin \frac{\theta}{2}$. Since each foil has its own inlet and exit region, there is a net moment on the fluid within each foil of magnitude $T_o r_o \left(\frac{6\mu U}{T_o}\right)^{2/3} \left(H_i - H_e\right)$, and the resultant foil force on the fluid (of magnitude P_o) cannot act through the shaft center but must be displaced by an amount δ (see Fig. A-9) where

$$P_o \cdot \delta = T_o r_o \left(\frac{6\mu U}{T_o}\right)^{2/3} \left(H_i - H_e\right)$$

The summation of the three-foil reactions on the fluid gives no net force but a couple of magnitude $3P_o\delta$. By symmetry, the center of the shaft must still be at the origin. However, the line of action of the resultant force of each foil on the fluid has been shown to have undergone a parallel displacement δ from the origin. This means that the asymptotes of the foil will have to adjust their position correspondingly.

Next consider the response to loading the shaft by an amount W in direction α (see Fig. A-9). Assume that the center of the shaft is displaced in steady state of (x, y). For the foil k, one finds

$$P_k \delta_k = T_k r_o \left(\frac{6\mu U}{T_k}\right)^{2/3} \left(H_i - H_e\right) \qquad (k = 1, 2, 3) \qquad \text{(A-20)}$$

$$P_k = 2T_k \sin\frac{\theta}{2} \qquad (k=1,2,3) \tag{A-21}$$

$$h_k^* - h_0^* = r_0 H^* \left\{ \left(\frac{6\mu U}{T_k}\right)^{2/3} - \left(\frac{6\mu U}{T_0}\right)^{2/3} \right\} \tag{A-22}$$

$$= -\frac{2}{3} r_0 H^* \left(\frac{6\mu U}{T_0}\right)^{2/3} \frac{T_k - T_0}{T_0} + \cdots \quad (k=1,2,3)$$

Using the notation $g(\theta) = \frac{\theta}{2} \sin\frac{\theta}{2} + \cos\frac{\theta}{2}$, it is found that for inextensible foil

$$\begin{aligned} q(\theta)(h_1^* - h_0^*) &= y \\ q(\theta)(h_2^* - h_0^*) &= -\frac{y}{2} - \frac{\sqrt{3}x}{2} \\ q(\theta)(h_3^* - h_0^*) &= -\frac{y}{2} + \frac{\sqrt{3}x}{2} \end{aligned} \tag{A-23}$$

Equilibrium requires

$$-P_2\frac{\sqrt{3}}{2} + P_3\frac{\sqrt{3}}{2} = -W\cos\alpha \tag{A-24}$$

$$P_1 - \frac{P_2}{2} - \frac{P_3}{2} = W\sin\alpha$$

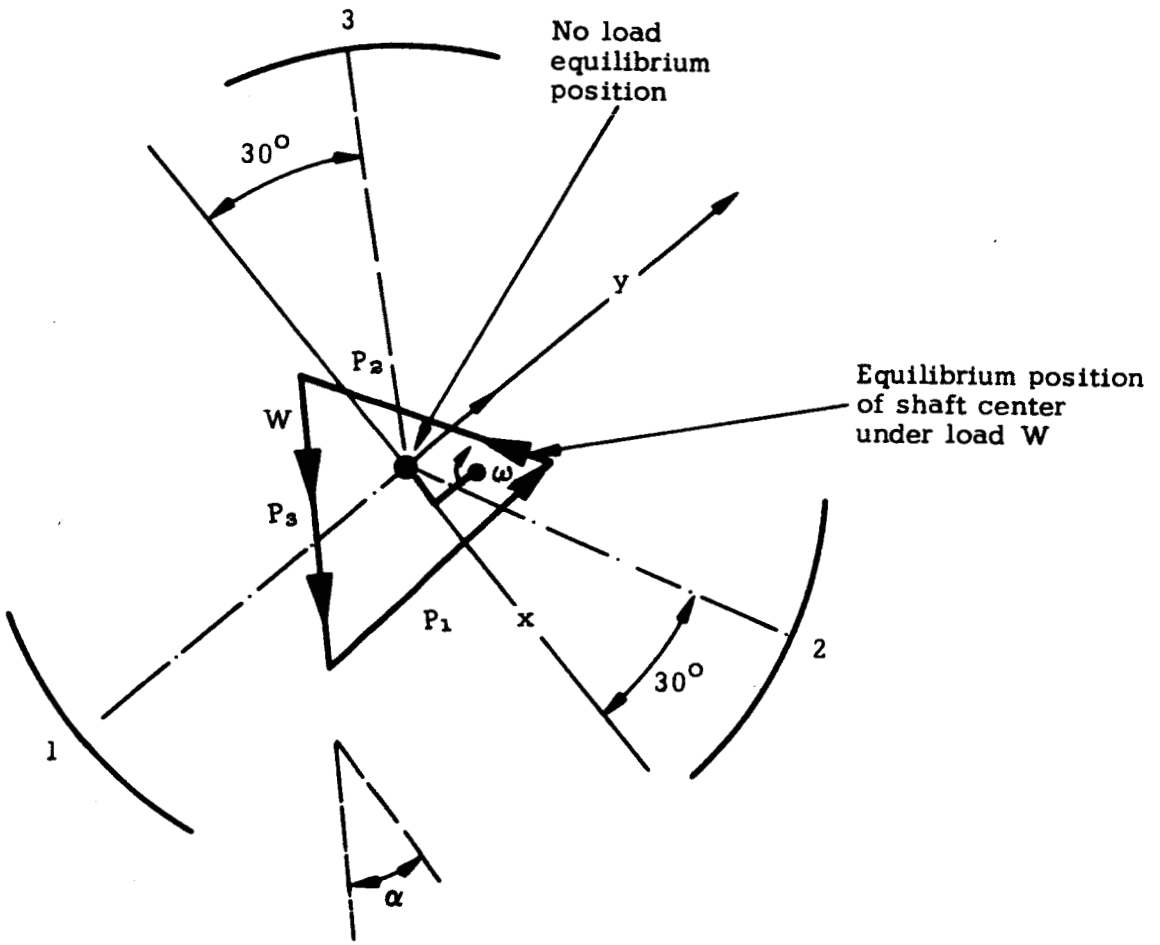

Fig. A-9 Three-Foil System

This set of equations allows the evaluation of the position of the shaft (x,y), the nominal clearances h_k^*, the tension T_k, the reaction forces P_k, and their lines of action $_k$.

Using the linearized form of Eq. (A-22) it is found that the displacement in the direction of the load

$$\delta_W = -y \sin\alpha + x \cos\alpha = \frac{2}{9} \frac{W r_o H^*}{\sin\frac{\theta}{2}} \left(\frac{6\mu U}{T_o}\right)^{2/3} g(\theta) \qquad \text{(A-25)}$$

and the displacement normal to the load is

$$\delta_H = x \sin\alpha + y \cos\alpha = 0 \qquad \text{(A-26)}$$

It follows that to a first approximation the attitude angle of the three-foil system is zero.

REFERENCES

1. W. A. Gross, Gas Film Lubrication, John Wiley and Sons, Inc., New York, 1962

2. B. Sternlicht, "Influence of Bearings on Rotor Behavior," Proceedings, International Symposium on Lubrication and Wear, edited by D. Muster and B. Sternlicht, McCutchen Publishing Corp., Berkeley, California, 1965, p 613

3. K. S. Lion, "Nonlinear Twin T Network for Capacitive Transducers," Review of Scientific Instruments, Vol. 35, No. 3, March 1964

4. A. Eshel and H. G. Elrod, Jr., "Theory of the Infinitely Wide, Perfectly Flexible, Self-Acting Foil Bearing," Paper No. 65-LUBS-3, ASME Spring Lubrication Symposium, 1965, New York, New York

5. H. K. Baumeister, "Further Considerations on the Nominal Clearance of the Foil Bearing," ASLE Paper 5B 5, 1964

6. O. Pinkus and B. Sternlicht, Theory of Hydrodynamic Lubrication, McGraw-Hill Book Company, Inc., New York, 1961